

# Iodine oxoacids and their roles in sub-3 nanometer particle growth in polluted urban environments

Ying Zhang<sup>1,2,3,\*</sup>, Duzitian Li<sup>2,3,\*</sup>, Xu-Cheng He<sup>4,5</sup>, Wei Nie<sup>2,3</sup>, Chenjuan Deng<sup>6</sup>,  
Runlong Cai<sup>4</sup>, Yuliang Liu<sup>2,3</sup>, Yishuo Guo<sup>1</sup>, Chong Liu<sup>2,3</sup>, Yiran Li<sup>6</sup>, Liangduo Chen<sup>2,3</sup>,  
5 Yuanyuan Li<sup>2,3</sup>, Chenjie Hua<sup>1</sup>, Tingyu Liu<sup>1</sup>, Zongcheng Wang<sup>1</sup>, Jiali Xie<sup>1</sup>, Lei Wang<sup>2,3</sup>,  
Tuukka Petäjä<sup>4</sup>, Federico Bianchi<sup>4</sup>, Ximeng Qi<sup>2,3</sup>, Xuguang Chi<sup>2,3</sup>, Pauli Paasonen<sup>4</sup>,  
Yongchun Liu<sup>1</sup>, Chao Yan<sup>2,3</sup>, Jingkun Jiang<sup>6</sup>, Aijun Ding<sup>2,3</sup>, Markku Kulmala<sup>1,2,3,4</sup>

<sup>1</sup>Aerosol and Haze Laboratory, Beijing Advanced Innovation Center for Soft Matter Science and Engineering, Beijing University of Chemical Technology, Beijing, China

10 <sup>2</sup>Joint International Research Laboratory of Atmospheric and Earth System Sciences, School of Atmospheric Sciences, Nanjing University, Nanjing, China

<sup>3</sup>Jiangsu Provincial Collaborative Innovation Center of Climate Change, Nanjing, China

<sup>4</sup>Institute for Atmospheric and Earth System/Physics, Faculty of Science, University of Helsinki, Helsinki, Finland

15 <sup>5</sup>Yusuf Hamied Department of Chemistry, University of Cambridge, Cambridge, CB2 1EW, UK

<sup>6</sup>State Key Joint Laboratory of Environment Simulation and Pollution Control, State Environmental Protection Key Laboratory of Sources and Control of Air Pollution Complex, School of Environment, Tsinghua University, Beijing, China

20 \*These authors contributed equally to this work.

*Correspondence to:* Xu-Cheng He (xucheng.he@helsinki.fi) and Wei Nie (niewei@nju.edu.cn)

**Abstract.** New particle formation contributes significantly to the number concentration of ultrafine  
25 particles (UFP,  $d \leq 100$  nm), and have great impacts on human health and global climate. Iodine oxoacids  
( $\text{HIO}_x$ , including iodic acid,  $\text{HIO}_3$  and iodous acid,  $\text{HIO}_2$ ) have been observed in pristine regions and  
proved to dominate NPF at some sites. However, the knowledge of  $\text{HIO}_x$  in polluted urban areas is rather  
limited. Here, we conducted a long-term measurements of gaseous iodine oxoacids and sulfuric acid in  
Beijing from January 2019 to October 2021 and also in Nanjing from March 2019 to February 2020, and  
30 investigated the contribution of  $\text{HIO}_x$  to UFP number concentration in both urban environments.  $\text{HIO}_3$  is  
highest in summer, up to  $2.85 \times 10^6 \text{ cm}^{-3}$  and  $2.78 \times 10^6 \text{ cm}^{-3}$  in Beijing and Nanjing, respectively, and is  
lowest in winter by 96% and 75%, respectively.  $\text{HIO}_3$  exhibits more prominent variation than  $\text{H}_2\text{SO}_4$  in  
both urban sites.  $\text{HIO}_3$  concentration shows a clear diurnal pattern at both sites with a daily maximum at

around noontime, similar to the atmospheric temperature, solar radiation and ozone ( $O_3$ ) levels.  $HIO_2$   
35 concentration has the same diurnal and seasonal trend as  $HIO_3$  but is overall about one order of magnitude  
lower than  $HIO_3$  concentration. Back trajectory analysis suggests that the sources for inland iodine  
species could be a mix of marine and terrestrial origins, both having peak iodine emission in warm  
seasons. While the contribution of  $HIO_2$  to particle growth is marginal in Beijing and Nanjing, our results  
demonstrate that  $HIO_3$  enhances the particle survival probability of sub-3 nm particles by about 40%  
40 (median) and occasionally by more than 100% in NPF events, suggesting  $HIO_x$  are significant contributor  
to UFPs in polluted urban areas. As the growth contribution from  $HIO_3$  and  $H_2SO_4$  is similar on a per-  
molecule basis, we propose that the sum of  $HIO_3$  and  $H_2SO_4$  could be used to estimate sub-3 nm particle  
growth of inorganic acid origin, in the polluted atmospheres with a significant amount of  $HIO_x$ .

## 1 Introduction

45 Aerosol particles are ubiquitous in Earth's atmosphere and have both primary and secondary sources  
(Kulmala et al., 2004b). Primary aerosol emissions stem from natural sources, including sea spray, soil  
mineral dust, biomass burning, and volcanic debris (Claudio Tomasi, 2017) and anthropogenic sources  
such as fuel combustion, industrial processes and transportation (Claudio Tomasi, 2017). Besides direct  
emissions, atmospheric new particle formation (NPF), a secondary particle source, plays a significant  
50 role in increasing aerosol population (Kulmala et al., 2012). Only a few vapours, such as sulfuric acid  
( $H_2SO_4$ ), water vapour ( $H_2O$ ), ammonia ( $NH_3$ ), amines (e.g., dimethylamine,  $C_2H_7N$ ) and highly  
oxygenated organic molecules (HOMs), are widely confirmed to nucleate and form new particles under  
appropriate atmospheric conditions (Kulmala et al., 2004a; Kürten et al., 2016; Li et al., 2020; Almeida  
et al., 2013; Kirkby et al., 2011; Kirkby et al., 2016; Lehtipalo et al., 2018; Tröstl et al., 2016; Yao et al.,  
55 2018). Once growing past the critical sizes (e.g., 50 nm to 100 nm), these newly formed particles can be  
activated as cloud condensation nuclei (CCN), which in turn influence cloud formation and have climatic  
effects (Kerminen et al., 2005; Kalkavouras et al., 2019; Jiang et al., 2021). Additionally, NPF is a  
dominant source of atmospheric ultrafine particles in polluted urban environments (Yan et al., 2021).  
These small particles ( $\leq 100$  nm) can penetrate into the respiratory system, thus posing health risks to  
60 human beings (Chen et al., 2016; Downward et al., 2018). Therefore, understanding NPF is important

both in terms of evaluating climate change and understanding the health risks of aerosols (Kulmala et al., 2022).

Due to its chemically complex nature, the understanding of the key precursor vapours and controlling mechanisms of urban NPF is still limited. Gaseous sulfuric acid and dimethylamine (DMA, C<sub>2</sub>H<sub>7</sub>N) are believed to play important roles in aerosol nucleation in urban environments (Xiao et al., 2021; Cai et al., 2021d; Almeida et al., 2013; Cai et al., 2022b; Yao et al., 2018). A recent study quantitatively demonstrated the decisive role of H<sub>2</sub>SO<sub>4</sub> in initiating nucleation with the presence of stabilisers such as amines and NH<sub>3</sub> in Beijing (Yan et al., 2021). The subsequent growth of fresh particles is contributed both by H<sub>2</sub>SO<sub>4</sub> and oxidised organic vapours depending on the particle sizes. In Beijing, it was suggested that H<sub>2</sub>SO<sub>4</sub> and its clusters contribute significantly to the growth of 1.5-3 nm particles (Deng et al., 2020b) while gas-phase oxygenated organic molecules (OOMs) promote the growth of 3-25 nm particles (Qiao et al., 2021).

Besides these widely studied species, oxidized iodine compounds were also found to introduce rapid particle formation, mostly observed in mid-latitude coastal sites (Hoffmann et al., 2001; Mäkelä, 2002; O'Dowd et al., 2002). Iodine nucleation was conventionally thought to be initiated by iodine oxides (Jimenez, 2003; Gomez Martin et al., 2020; O'Dowd and Hoffmann, 2005; Hoffmann et al., 2001; O'Dowd et al., 2002). However, field observations at the Mace Head observatory and dedicated experiments carried out in the CLOUD chamber at CERN revealed iodine oxoacids (HIO<sub>x</sub>, i.e., HIO<sub>3</sub> and HIO<sub>2</sub> in this study) as the key nucleating species in pristine regions (Zhang et al., 2022; He et al., 2021b). With state-of-the-art mass spectrometric methods, iodine oxoacids were recently identified in locations other than mid-latitude coastal sites, such as in Arctic sites (Baccarini et al., 2020; Beck et al., 2021; Sipilä et al., 2016; He et al., 2021b), Antarctica sites (Jokinen et al., 2018; He et al., 2021b), boreal forest sites (Jokinen et al., 2022; He et al., 2021b), a remote marine site (He et al., 2021b) and importantly also in polluted urban sites (He et al., 2021b). Chamber experiments have shown that HIO<sub>3</sub> (stabilized by HIO<sub>2</sub>) nucleates faster than H<sub>2</sub>SO<sub>4</sub> with 100 pptv NH<sub>3</sub> at the same temperature and equal acid concentrations, although iodine oxoacid nucleation rates are still lower than H<sub>2</sub>SO<sub>4</sub>-DMA nucleation (He et al., 2021b). It is worthwhile to note that the nucleation involving both iodine oxoacids and DMA remains unclear and iodine oxoacid nucleation may further be enhanced by strong bases (e.g., different amines) in urban environments. After the formation of fresh particles, HIO<sub>3</sub> dominates the growth of iodine particles

between 1.8 and 3.2 nm at growth rates equal to those of H<sub>2</sub>SO<sub>4</sub> (He et al., 2021b). It can be expected that, iodine oxoacids will contribute at least to sub-3 nm particle growth, and potentially also to particle nucleation, in polluted urban environments. Therefore, iodine oxoacids have the potential to enhance the survival probability (Lehtinen et al., 2007) of fresh particles in the urban environment.

95

In order to quantitatively understand the contribution of iodine oxoacids in urban particle formation, we conducted a long-term measurement of iodine oxoacids and sulfuric acid (H<sub>2</sub>SO<sub>4</sub>) in urban Beijing from January 2019 to October 2021, and in suburban Nanjing from March 2019 to February 2020. Diurnal and seasonal trends of iodine and sulfur oxoacids are analysed and the potential sources of the unexpected iodine oxoacids are discussed. Moreover, we quantitatively discuss the contribution of HIO<sub>3</sub> to aerosol growth rate below 3 nm (GR<sub><3nm</sub>) and the potential enhancement in particle survival probability. Our study provides the first long-term observations of iodine oxoacids in polluted urban environments which could contribute to aerosol formation studies in inland cities.

100

## 2 Methods

105

### 2.1 Measurement sites and instruments

#### 2.1.1 Sites

110

Measurements in urban Beijing were conducted from January 2019 to October 2021, on the fifth floor of the teaching building at the west campus of Beijing University of Chemical Technology (Aerosol and Haze Laboratory (AHL)/BUCT station, 39 ° 56'N, 116 ° 17'E). Located about 150 km away from the nearest coastline in the southeast, the station is surrounded by residential buildings and three main roads and a detailed description of this site can be found in a previous study (Liu et al., 2020). The observations in Nanjing were conducted at the Station for Observing Regional Process of Earth System (SORPES; 118°57'E, 32°07'N), a research and experiment platform inside Nanjing University, Xianlin Campus, 20 km northeast of downtown Nanjing and about 190 km away from the nearest coastline in the east.

115

Because of its unique geophysical location, the SORPES is considered to be a regional background station under the influence of anthropogenic plume from YRD (Yangtze River Delta) city cluster and multiscale transport coupled with Asian monsoon (Ding et al., 2016). The geophysical distribution of two sites can be found in Fig. S1.

### 2.1.2 Acid concentrations

120 Gaseous iodine oxoacids ( $\text{HIO}_3$  and  $\text{HIO}_2$ ) and  $\text{H}_2\text{SO}_4$  were detected by the nitrate-CIMS (Aerodyne Research Inc. and Tofwerk AG) composed of a chemical ionization (CI) source and an atmospheric pressure interface time-of-flight mass spectrometer (API-TOF). Two long time-of-flight mass analysers (LToF, resolution at around 10,000 Th  $\text{Th}^{-1}$ ) were used at the AHL/BUCT station from January 2019 to October 2021 and at SORPES station from March 2019 to December 2019, respectively, while a lower resolution time-of-flight analyser (HToF, resolution at around 5,000 Th  $\text{Th}^{-1}$ ) was utilized at the SORPES station from January 2020 to February 2020. As the comprehensive description of nitrate-CIMS has been given in previous works (Junninen et al., 2010; Jokinen et al., 2012), they are only briefly discussed here. Ambient air was drawn into a laminar flow reactor through a 0.75 in. diameter stainless steel tube with a sample flow of about 7.2 L/min and surrounded by a purified airflow of 32 L/min serving as the sheath

125 flow at the AHL/BUCT station and 25 L/min at the SORPES station. The dominant reagent ions were nitrate ions ( $\text{NO}_3^-$  and  $\text{HNO}_3 \cdot \text{NO}_3^-$  and  $\text{HNO}_3\text{HNO}_3 \cdot \text{NO}_3^-$ ), which were generated in the sheath flow by exposing gaseous nitric acid in the sheath flow to a photo ionizer X-ray (Model L9491, Hamamatsu, Japan). The data of nitrate-CIMS were acquired at 1 Hz time resolution and analysed with the MATLAB (MathWorks Inc.) toolbox ToFTools package (version 6.11) (Junninen et al., 2010).

135  $\text{H}_2\text{SO}_4$  calibration was conducted using a standardized method (Kurten et al., 2012; He et al., 2023). In a nutshell, the calibration of  $\text{H}_2\text{SO}_4$  involved the reaction of an excessive amount of sulfur dioxide ( $\text{SO}_2$ ) with a known quantity of hydroxyl (OH) radicals generated by a portable mercury lamp. This mercury lamp is equipped with a filter to intercept the sample air containing water, which, in turn, is photolyzed to produce OH radicals. The convection-diffusion-reaction processes within the chemical ionization inlet

140 can be accurately simulated using a two-dimensional model (e.g., the MARFORCE-Flowtube model) (He et al., 2023), allowing for the quantification of  $\text{H}_2\text{SO}_4$  concentration at the mass spectrometer's entrance. The quantification of the measured signals for  $\text{H}_2\text{SO}_4$  monomer at both sites are seasonal calibrated with diffusion losses in tube into consideration. Since both  $\text{H}_2\text{SO}_4$  and  $\text{HIO}_x$  are detected at the collision limit, they share the same calibration factor (He et al., 2021b; He et al., 2023). The general

145 systematic error for the detection of  $\text{H}_2\text{SO}_4$  and  $\text{HIO}_x$  is expected to be within 50% to 200% (Liu et al., 2021).

### **2.1.3 Particle number size distribution**

The particle number size distribution (PNSD) from approximately 1 nm to 10  $\mu\text{m}$  at the AHL/BUCT station was measured. This was done using a diethylene glycol scanning mobility particle spectrometer (DEG-SMPS, 1-4.5 nm) (Jiang et al., 2011), equipped with a miniature cylindrical differential mobility analyzer (mini-cy DMA) (Cai et al., 2017a). In addition, we utilized a homemade particle size distribution system (PSD, 3 nm-10  $\mu\text{m}$ ) (Liu et al., 2016). At the SORPES station, the PNSD was measured using an Aerodynamic Particle Sizer (APS, TSI, APS-3321, USA, 500-1000 nm) and two SMPSs equipped with a TSI long-DMA (TSI Inc., model 3081) and a TSI nano-DMA (TSI Inc., model 3085). Additionally, ions of sizes range from 0.8 nm to 42 nm were measured using a Neutral cluster and Air Ion Spectrometer (NAIS, Airel Ltd., Estonia) (Manninen et al., 2016) in Nanjing.

### **2.1.4 O<sub>3</sub> concentration and other meteorological factors**

The ozone (O<sub>3</sub>) concentration was measured using ozone analysers (49i, Thermo Fisher Scientific Inc. USA) at both sites. Additionally, ambient meteorological factors, including temperature (T), relative humidity (RH), and ultraviolet B radiation (UVB) were measured using an Automatic Weather Station (AWS310, Vaisala Inc.) in Beijing, whereas T, RH, and downward short-wave radiation (DSR) were recorded by sensors at the height of 44 m above the ground level at the SORPES station. The T and RH were measured by a temperature and relative humidity probe (HMP155A, Campbell Inc., USA), and the DSR was recorded by a CNR4 net radiometer (OTT Hydromet Corp. Germany).

## **2.2 Data analysis**

### **2.2.1 Characteristic of NPF events from PNSD**

According to a widely used method (Kulmala et al., 2012), we classified all of the measurement days into NPF and non-NPF events at both sites. All undefined days were regarded as non-NPF events in this study. Furthermore, NPF events exhibiting obvious nucleation and clear growth of fresh nucleation particles were categorized as "NPF-A," while the remaining NPF events were designated as "NPF-B". Since there were periods when some key instruments failed to work, the NPF frequencies in each month were calculated as the ratio of the NPF event days to the days with valid data. The monthly statistics at both sites were summarized in Table S1. From the measured particle number size distribution, we

calculated the condensation sink (CS) (Laakso et al., 2004; Kulmala et al., 2012), coagulation sink  
 175 (CoagS) (Kulmala et al., 2001), and growth rate (GR) for the NPF events.

CS, which characterises the loss rate of gaseous precursors and clusters onto the particles (Lehtinen et  
 al., 2003) was calculated using the equation Eq. (1) (Kulmala et al., 2012):

$$180 \quad CS = 4\pi D \sum_j \frac{1}{2} d_{p,j} \beta_m(Kn_j, \alpha) N_j , \quad (1)$$

where,  $D$  is the  $H_2SO_4$  vapour diffusion coefficient;  $d_{p,j}$  is particle diameter;  $\beta_m$  is transitional  
 correction factor for mass flux (Fuks and Sutugin, 1970) as a function of  $Kn_j$  (Knudsen number) and  $\alpha$   
 (mass accommodation coefficient, assumed to be unity in this work) as shown in Eq. (2);  $N_j$  is the  
 185 number concentration of  $d_{p,j}$ , and the particle diameter is corrected for growth factor according to T and  
 RH (Laakso et al., 2004).

$$\beta_m = \frac{1+Kn_j}{1+0.377Kn_j+1.33Kn_j(1+Kn_j)/\alpha} , \quad (2)$$

190 To quantify if notable growth is to occur, especially for sub-3 nm particles, it is crucial to understand the  
 loss process of fresh particles. Coagulation scavenging of freshly formed particles into pre-existing  
 particles before growing to significant sizes is essential for estimating the concentration of newly  
 nucleated particles at the size of 1.5-2 nm (Kulmala et al., 2001). Aerosol coagulation sink (CoagS)  
 represents this kind of coagulated scavenging characteristics. CoagS (the loss through coagulation among  
 195 particles) was determined from Eq. (3). Here,  $K_{ij}$  is the coagulation coefficient (Kulmala et al., 2001).

$$CoagS = \sum_j K_{ij} N_j , \quad (3)$$

Besides, the GRs in NPF events were determined with both the appearance time method (including APT-  
 200  $x$  and APT- $y$ ) and the mode fitting method (MOD) to minimize the uncertainty from calculations (Dada  
 et al., 2020; Kulmala et al., 2012). Detailed approach is shown in supplementary materials. The size-  
 segregated GRs were calculated in two size ranges, i.e., sub-3 nm ( $GR_{<3}$ ) and 3-7 nm ( $GR_{3-7}$ ) based on

the appearance time method, and the 50% appearance time is fitted by smoothing the normalized concentration timeseries for the particle of each size bin (Lehtipalo et al., 2014; He et al., 2021a). After  
 205 determining the 50% appearance time for each size bin, the GRs were fitted using the linear least square method both with time as  $x$  and  $y$  to compare with each other and minimize the error. They are referred to as APT- $x$  and APT- $y$ , respectively in this study. The slope of particle size to their 50% appearance time was regarded as GR using APT- $x$ , which is the traditional way. However, as the particle diameter is exactly measured by our instruments and the 50% appearance time is the independent variable  
 210 determined by calculations, we also tried to use the latter as the independent variable to fit the GR. In this case, the GR was determined as the inverse of the fitted slope. The mode fitting (MOD) method fits the particle number size distribution to find the mode diameters at any given time and tracks the evolution of particle sizes. Up to now, there is still a debate about whether to adopt the appearance time method or the mode fitting method for GR calculation, as neither is perfect for calculating GR for ambient  
 215 observations (Qiao et al., 2021; Deng et al., 2020b). For example, it is difficult to define the accurate mode diameter, especially for sub-3 nm particles when the new particle formation just occurs. Therefore, there could be some underestimation while using mode fitting method to calculate  $GR_{<3}$  (Cai et al., 2022a). Determining the sub-3 nm particle growth can also be difficult for the 50% appearance time method for similar reasons. Additionally, appearance time method might be more sensitive to other  
 220 processes as it does not track the growth of a particle or a population. (Lehtipalo et al., 2014; Cai et al., 2021c; He et al., 2021a). In this study, we report results using both methods to reduce the overall uncertainty of GR calculation and to provide a confidence range of GR. In both cases, the GR is determined from the rate of change in diameter shown as Eq. (4) (Kulmala et al., 2012).

$$225 \quad GR = \frac{dd_p}{dt} , \quad (4)$$

It is worthwhile to note that we corrected the GR obtained from the 50% appearance time method for the impact of coagulation sink, following Eq. (5) (Cai et al., 2021c).

$$230 \quad GR_{corr,cond} = GR_{conv} - \left( CoagS + \frac{CoagSrc}{2N_p} \right) \times \left[ \sqrt[3]{(d_p^3 + d_1^3)} - d_p \right] - GR_{coag} , \quad (5)$$



where the  $GR_{conv}$  is the GR calculated from conventional appearance time method in  $\text{nm}\cdot\text{s}^{-1}$ ;  $CoagSrc$  is the coagulation source defined as the production rate of the particle size bin because of coagulation,  $\text{cm}^{-3}\text{s}^{-1}$ , calculated using the Eq. (6);  $N_p$  is the number concentration of particles with the size  $d_p$ ;  $GR_{coag}$  is the coagulation growth rate in  $\text{nm}\cdot\text{s}^{-1}$  from Eq. (7). More specific details can be found in Cai et al. (2021c).

$$CoagSrc = 0.5 \times \iint_{\substack{d_i^3+d_j^3 \leq d_{p,u}^3 \\ d_{p,1}^3 \leq d_i^3+d_j^3}} \beta_{i,j} n_i n_j \times d \log d_i \times d \log d_j, \quad (6)$$

$$GR_{coag} = \sum_{d_p=d_{min}}^{d_p=d_p} \left\{ \beta_{p,i} N_i \times \left[ \sqrt[3]{(d_p^3 + d_i^3)} - d_p \right] \right\}, \quad (7)$$

240

The counterbalance of CoagS and GR considerably affects the survival of small clusters (Mahfouz and Donahue, 2021). Survival probability (SP) is utilized to quantify the competition between growth and scavenging mentioned above (Veli-Matti Kerminen, 2002; Kerminen et al., 2005). We defined the  $SP_{1.5-3}$  and  $SP_{3-7}$  as the likelihood that the particles can grow from the smaller sizes to the larger sizes (i.e., from 1.5 to 3 nm and from 3 to 7 nm, respectively) before they are scavenged by coagulation. The SP can be calculated following Eq. (8) (Lehtinen et al., 2007).

245

$$SP = \exp \left\{ \frac{d_{p1}}{m-1} \frac{CoagS}{GR} \left[ \left( \frac{d_{p2}}{d_{p1}} \right)^{1-m} - 1 \right] \right\}, \quad (8)$$

250 where  $d_{p1}$  and  $d_{p2}$  are the lower limit size and upper limit size, respectively; CoagS is the coagulation sink at the lower limit size; GR is the averaged growth rate in the size range, from both corrected appearance time method and mode fitting method;  $m$  was assumed to be 1.7 according to the measured PNSDs (Lehtinen et al., 2007).

### 255 2.2.2 Contribution of HIO<sub>3</sub> to GR and SP

To better understand the role of HIO<sub>3</sub> as an additional GR contributor at two sites, we calculate the condensational GR of HIO<sub>3</sub> and H<sub>2</sub>SO<sub>4</sub> during NPF events, the computation criteria are listed as below. The particle growth rate due to HIO<sub>3</sub> concentration was observed to be linear in the CLOUD experiment, shown as Eq. (9), which is fitted at 10 °C (He et al., 2021b):

260  $GR(\text{HIO}_3)_{1.8-3.2} = 10^{\log_{10}[\text{HIO}_3]-6.75}$  , (9)

where  $[\text{HIO}_3]$  is the iodic acid concentration in molecules  $\text{cm}^{-3}$  and  $GR(\text{HIO}_3)_{1.8-3.2}$  is the growth rate of 1.8 to 3.2 nm particles in  $\text{nm h}^{-1}$ . However, the size range of sub-3 nm particles used in this study (1.5 to 3 nm) slightly differs from 1.8 to 3.2 nm and this formulation does not provide the growth rates of 3 to 7 nm particles. Additionally, as the temperature in summer seasons in both Beijing and Nanjing  
 265 (around 22 to 36 °C) is much higher than 10 °C, additional temperature correction is needed. In this study, we adopt the equation provided by Nieminen et al. (2010) for these corrections:

$$GR'(\text{HIO}_3) = \frac{\Delta d_p}{\Delta t} = \frac{\Delta d_p \text{HIO}_3 \alpha_m m_v}{2\rho_v d_p} \cdot \sqrt{\frac{8kT}{\pi m_v}} \cdot \frac{1}{\left[ \frac{2x_1+1}{x_1(x_1+1)} - \frac{2x_0+1}{x_0(x_0+1)} + 2\ln\left(\frac{x_1(x_0+1)}{x_0(x_1+1)}\right) \right]} , \quad (10)$$

270 where the subscript “v” refers to  $\text{HIO}_3$ . Additionally,  $x_0$  and  $x_1$  are the ratios of the diameter of  $\text{HIO}_3$  molecule divided by the particle diameter at which the initial growth occurs (e.g., 1.5 nm or 1.8 nm) and particle diameter at which the particles grow to (e.g., 3 nm or 3.2 nm), respectively. Two sets of growth rates were calculated using this equation: 1) the first set utilized the measured ambient temperature at the given growth period of NPF events with 1.5 to 3 nm or 3 to 7 nm as the growth ranges and 2) the second  
 275 set calculated the growth rates at 10 °C with 1.8 to 3.2 nm as the growth range (the same as at CLOUD). The ratios of the growth rates calculated by 1) and 2) therefore give the correction factors that can be applied to Eq. (9) to correct the temperature and size differences. The correction factors, determined by analyzing temperature measurements at two sites and selected size ranges on NPF event days, remained consistently close to 1 (as shown in Fig. S2 for more detailed information). This suggests that the  
 280 variations in size range and temperature between the CLOUD measurements and our field observations are minimal.

To quantify the growth rates of particles with mean diameter from around 1 nm to 7 nm in Nanjing, the negative ion number size distribution collected by NAIS was utilized. However, it is extremely difficult  
 285 to use the NAIS to capture sub-3 nm particle growth rates as the limited atmospheric ions are mostly captured by larger particles in polluted urban environments and thus leaving the sub-3 nm particle growth undetectable (see supplementary materials for details). Therefore, in all NPF cases occurred at the SORPES station, the contribution of gaseous iodic acid to sub-3 nm growth is only quantified by

comparing its contribution with that of sulfuric acid during the same event, since H<sub>2</sub>SO<sub>4</sub> is believed to be  
 290 the significant contributor to particle initial growth in sub-3 nm range (Deng et al., 2020b).

$$GR(\text{H}_2\text{SO}_4) = (2.68 \times d_p^{-1.27} + 0.81) \times ([\text{H}_2\text{SO}_4] \times 10^{-7}) , \quad (11)$$

H<sub>2</sub>SO<sub>4</sub> contribution to GR is calculated as a first-order approximation independent of temperature as Eq.  
 (11) (Stolzenburg et al., 2020), where  $d_p = \frac{d_{p\text{initial}} + d_{p\text{final}}}{2}$  in nm, and the subscripts initial and final  
 refer to the particle diameter at the beginning and the end of the growing process. [H<sub>2</sub>SO<sub>4</sub>] is the gas  
 295 phase H<sub>2</sub>SO<sub>4</sub> concentration in molecule cm<sup>-3</sup>. But it should be noted that H<sub>2</sub>SO<sub>4</sub> does not dominate alone  
 the initial growth process, other organic species may make some contribution as well. Therefore, in this  
 study, the results calculated at SORPES is disadvantaged compared to the BUCT/AHL data using directly  
 measured GRs. This part of the results should be considered a compromise due to the absence of direct  
 measurements.

300 We define SP<sub>tot</sub> as the particle survival probability calculated using the measured GRs (in Beijing) or the  
 expected growth rate considering growth contributions from both H<sub>2</sub>SO<sub>4</sub> and HIO<sub>3</sub> (in Nanjing). In order  
 to quantify the SP enhancement by HIO<sub>3</sub>, we further define SP<sub>1</sub> which represents the calculated survival  
 probability using GRs after deducting the growth contribution from HIO<sub>3</sub>. Therefore, the enhancement  
 factor (EF) of SP can be represented as

$$EF = \frac{SP_{tot}}{SP_1} - 1 . \quad (12)$$

### 2.2.3 Iodic acid (HIO<sub>3</sub>) precursor proxy

In order to investigate the source of gaseous HIO<sub>3</sub> at both sites, a daytime proxy formula is built to  
 310 describe the precursor level of measured HIO<sub>3</sub>, which is as follows:

$$Proxy_{pre} = \frac{[\text{HIO}_3] \times CS}{UVB} \quad (13)$$

Eq. (13) is derived by assuming the HIO<sub>3</sub> concentration to be at a pseudo-steady state (the production  
 rate equals to the loss rate). Based on current knowledge about HIO<sub>3</sub> formation pathways, the proxy is  
 not intended to elucidate the composition of species serving as HIO<sub>3</sub> precursor or the related reactions.  
 315 Instead, it considers the photochemical reaction as the daytime formation pathway and condensation onto  
 pre-existing aerosol particles as the only sink for gaseous HIO<sub>3</sub>.

### 3 Results and Discussion

#### 3.1 Overview of the measurement

The measurement overviews in both Beijing and Nanjing are presented in Fig. 1, including the timeseries  
320 of T, O<sub>3</sub>, HIO<sub>x</sub> and H<sub>2</sub>SO<sub>4</sub> concentrations, as well as the frequency of NPF events in each month. It  
should be noted that each point on timeseries panels refers to daytime mean value. In this work, daytime  
duration is defined between 08:00 and 16:00 in local time (UTC+8) considering the preferred time  
window of NPF events in China (Kulmala et al., 2021), as shown in Fig. S3.

In Fig.1(a)/(d), it is obvious that the seasonal patterns of T and O<sub>3</sub> are similar during measurement periods  
325 in both sites, i.e., both peak in the summer. The O<sub>3</sub> levels are roughly the same at both sites and the  
maximum values of daily mean T are both over 35°C, though the lowest T (about 1°C) in Nanjing is  
significantly higher than that in Beijing (about -12°C).

H<sub>2</sub>SO<sub>4</sub> concentration is slightly lower in cold seasons (Fig.1(b)/(e)). H<sub>2</sub>SO<sub>4</sub> concentration exceeds 10<sup>7</sup>  
cm<sup>-3</sup> only on a few days in Beijing, whereas it is a common phenomenon in Nanjing daytime. Besides  
330 H<sub>2</sub>SO<sub>4</sub>, we report the first long-term measurement of HIO<sub>x</sub> in urban environments continued from earlier  
sparse measurements (He et al., 2021b). The calibrated HIO<sub>x</sub> concentration is above the detection limit  
during almost the entire measurement periods, indicating a clear presence of HIO<sub>x</sub> in inland cities. The  
HIO<sub>3</sub> concentration was between 10<sup>5</sup> and 10<sup>6</sup> cm<sup>-3</sup> for most of the time except for winter months; it  
sporadically approaches or is higher than 10<sup>6</sup> cm<sup>-3</sup> in warm months. On the other hand, iodosic acid, HIO<sub>2</sub>  
335 is less abundant than HIO<sub>3</sub> at both sites with a general concentration at around 10<sup>4</sup> cm<sup>-3</sup> and a maximum  
concentration approaching 10<sup>5</sup> cm<sup>-3</sup> in the summer. The results indicate that the H<sub>2</sub>SO<sub>4</sub> concentrations  
are generally higher than that of iodine oxoacids at both sites. The ratios of H<sub>2</sub>SO<sub>4</sub> to HIO<sub>3</sub> at both sites  
differ so slightly, with about 10% in Beijing and 9% in Nanjing, respectively. As for the two iodine  
oxoacids (HIO<sub>3</sub> and HIO<sub>2</sub>), daytime mean concentration of HIO<sub>3</sub> is more than one order of magnitude  
340 higher than HIO<sub>2</sub>. The one order of magnitude lower HIO<sub>3</sub> concentration compared with H<sub>2</sub>SO<sub>4</sub> in  
summer at both sites is consistent with that in the Finnish subarctic boreal forest (Jokinen et al., 2022).

The frequencies of NPF events varied significantly, from none to more than 75% of the days in each  
month during the measurement period. The occurrence of NPF events in China is favoured by various  
meteorological factors (Qi et al., 2015; Zhou et al., 2021; Chu et al., 2019). However, the influences can  
345 be quite uncertain and complex because of different season and the location of measurement site. Take

temperature for an example, on one hand, warm temperatures enhance the abundance of biogenic and anthropogenic volatile organic compound emissions as well as their oxidation processes (Paasonen et al., 2013; Paasonen et al., 2018; Nie et al., 2022; Ehn et al., 2014). On the other hand, the warm temperature also reduces the stability of embryonic clusters thus reducing nucleation and subsequent growth rates (Kürten et al., 2016). Besides meteorological conditions, vapour condensation sink (CS) and particle coagulation sink (CoagS) have negative effects on the NPF frequency (Kalkavouras et al., 2017; Bousiotis et al., 2021; Wehner et al., 2007). Decreased CS and/or CoagS will lead to faster nucleation and subsequent growth (as scavenging of nucleating and condensable vapours is less effective) and higher survival probability through the growth processes during NPF events (as the scavenging of clusters and small particles is less effective). As expected, the concentration of gaseous  $\text{H}_2\text{SO}_4$  is notably correlated with NPF frequency, as  $\text{H}_2\text{SO}_4$  is the most important compound to form initial clusters and one of the main contributors to the growth of newly formed particles (Nieminen et al., 2010; Kirkby et al., 2011). During this measurement, the ratio of  $\text{GR}_{1.5-3}$  contributed from  $\text{H}_2\text{SO}_4$  to measured GR calculated from MOD is about 72.4% (shown in Table S4).

360

As depicted in Fig. 1(c)/(f), the frequencies of NPF for each month at two sites are quite different, since environments are chemically complex and diverse with many aforementioned factors influencing NPF. Generally, NPF events are more likely to occur in the spring and winter, with the lowest frequency in summer at BUCT station in Beijing, consistent with other reports (Wu et al., 2007; Deng et al., 2020b). Different from Beijing, there are less NPF events in the winter than in the summer at SORPES station, which is in line with a long-term measurement conducted at the same site (Qi et al., 2015). It could be attributed to the lowest  $\text{H}_2\text{SO}_4$  concentration in cold season, which was found to be the main driver for NPF events in polluted megacities in China (Yao et al., 2018). Another explanation may be that the high CS in the winter daytime (Qi et al., 2015) suppresses the NPF events. It should be noted that the particle formation mechanism in Nanjing is yet to be revealed and NPF intensity could be reduced if DMA is limited in Nanjing.

370

## 3.2 Characteristic of acid concentrations

### 3.2.1 Seasonal variation

To better understand the roles of the studied acids in NPF, we further present the seasonal variation of H<sub>2</sub>SO<sub>4</sub>, HIO<sub>3</sub> and HIO<sub>2</sub> concentrations in Fig. S4. It depicts the monthly statistics of H<sub>2</sub>SO<sub>4</sub> and HIO<sub>x</sub> at the two sites with different shadings indicating seasons. Both H<sub>2</sub>SO<sub>4</sub> and HIO<sub>x</sub> concentrations in Nanjing are always higher than those in Beijing except for H<sub>2</sub>SO<sub>4</sub> concentrations in the winter. We speculate that the generally higher acid concentrations in Nanjing are caused by stronger solar radiation at latitude of 32°07'N in Nanjing, compared with 39°56'N in Beijing. On the other hand, the reason of higher wintertime H<sub>2</sub>SO<sub>4</sub> concentrations in Beijing is likely due to the higher SO<sub>2</sub> and more frequent sunny weather during the winter in Beijing (Wang et al., 2018) and further discussion can be seen in supplementary materials. At both sites, the seasonal pattern of H<sub>2</sub>SO<sub>4</sub> is not very strong (Deng et al., 2020b; Petäjä et al., 2009). H<sub>2</sub>SO<sub>4</sub> concentrations are higher in the spring and autumn, lower in the summer, and lowest in the winter. This variation of H<sub>2</sub>SO<sub>4</sub> in different seasons is determined by both its source and sink. Winter is characterized by the weakest solar radiation and the heaviest particle pollution, which collectively result in lowest H<sub>2</sub>SO<sub>4</sub> levels, whereas lower SO<sub>2</sub> concentrations in summer could limit H<sub>2</sub>SO<sub>4</sub> formation.

The HIO<sub>3</sub> concentrations measured at the two sites are significantly lower, approximately two orders of magnitude less than that at pristine coastal site (e.g., in Mace Head). Measurements at Mace Head indicate that HIO<sub>3</sub> concentrations are frequently above 10<sup>7</sup> cm<sup>-3</sup> with some days exceeding 10<sup>8</sup> cm<sup>-3</sup> in September. The concentrations of atmospheric iodine at coastal sites are normally higher due to active biogenic emissions of iodine-containing precursors from marine algae (O'Dowd et al., 2002). On the other hand, HIO<sub>3</sub> concentrations in Beijing and Nanjing are comparable to that in Helsinki, Finland. Measurements at SMEAR III station, an urban site located in University of Helsinki show HIO<sub>3</sub> concentrations at around 10<sup>6</sup> cm<sup>-3</sup> when the wind is coming from land for most times in August and HIO<sub>3</sub> concentrations exceed 10<sup>7</sup> cm<sup>-3</sup> when air masses have marine origin (Thakur et al., 2022; He et al., 2021b). Another long-term observation conducted at SMEAR I station (Jokinen et al., 2022), a subarctic boreal forest site, shows HIO<sub>3</sub> concentrations often at around 10<sup>5</sup> cm<sup>-3</sup> from April to November 2019 (summer and autumn) with occasional peaks exceeding 10<sup>6</sup> cm<sup>-3</sup> in late August. HIO<sub>x</sub> concentrations at AHL/BUCT station depict a distinctly unimodal pattern in a year cycle with highest values in July,

increasing from January and decreasing to December. However, seasonal variations of  $\text{HIO}_x$  are slightly different at SORPES, as there are similar levels of  $\text{HIO}_x$  throughout the summer in 2019, reaching a seemingly steady daily maximum.  $\text{HIO}_3$  concentration measured from August to September in 2018 over the central Arctic Ocean increases significantly from summer towards autumn (Baccarini et al., 2020),  
405 which is different from the results in both Beijing and Nanjing, due to significantly different environments and iodine sources.

### 3.2.2 Diurnal pattern

Though the  $\text{HIO}_3$  concentrations are different in four seasons, the diurnal patterns are similar throughout  
410 the year (Fig. 2). Daily trends of both median  $\text{H}_2\text{SO}_4$  and  $\text{HIO}_x$  concentration are strongly connected with diurnal cycle. The concentration of  $\text{HIO}_x$  increases at the same time as  $\text{H}_2\text{SO}_4$ , i.e., both  $\text{HIO}_x$  and  $\text{H}_2\text{SO}_4$  rise in the early morning and peak from noon to afternoon. The clear diurnal pattern of  $\text{H}_2\text{SO}_4$  has been attributed to photochemical activities (Lu et al., 2019; Yang et al., 2021; Petäjä et al., 2009). Hydroxyl radical (OH) is the most important oxidant for sulfur dioxide ( $\text{SO}_2$ ) to form daytime  $\text{H}_2\text{SO}_4$  (Guo et al.,  
415 2021; Yang et al., 2021). Therefore, the diurnal pattern of  $\text{H}_2\text{SO}_4$  would be affected by its precursors (e.g.,  $\text{SO}_2$  and OH in daytime). Higher  $\text{HIO}_x$  concentrations in the daytime and the absence of their nocturnal maxima suggest that the main source of  $\text{HIO}_x$  is also photochemical oxidation of iodine precursor vapours. As depicted in Fig. 2, this pronounced diurnal variation in  $\text{HIO}_x$  levels is consistently observed at both sites throughout the entire measurement period, regardless of the season. The peak concentrations of  
420  $\text{HIO}_x$  consistently exceed the minimum levels by a factor of approximately one order, with this difference being particularly significant, especially for  $\text{HIO}_3$  during summer. The distinct variation from day to night suggests that  $\text{HIO}_x$  formation is primarily occurring in situ, rather than being transported from other regions. Although the diurnal patterns of  $\text{H}_2\text{SO}_4$  and  $\text{HIO}_3$  are alike, the occurrence of  $\text{HIO}_3$  daytime maximum is on average later than that of  $\text{H}_2\text{SO}_4$  at both sites (Fig. 2). This phenomenon is pronounced  
425 regardless of season at both sites with the daily maximum of  $\text{H}_2\text{SO}_4$  appears around 1-2 hours earlier than that of  $\text{HIO}_3$ . It implies that albeit these two acids form during daytime through photochemical pathways, the limiting factors for their productions can be different. At the SORPES station, for instance, the diurnal cycle of  $\text{H}_2\text{SO}_4$  follow that of radiation. In summer, however, owing to effectiveness of long-term emission reduction,  $\text{SO}_2$  concentrations can be low enough to limit the production of  $\text{H}_2\text{SO}_4$  at

430 SORPES (Ding et al., 2019), so the daytime peaks of  $\text{H}_2\text{SO}_4$  tend to occur when  $\text{SO}_2$  reached its daily maximum (Yang et al., 2021). On the other hand, little is known about the diurnal patterns of  $\text{HIO}_x$  in urban environments. It was demonstrated in chamber experiments that  $\text{HIO}_x$  can be formed by oxidation of oxidised iodine species with ozone in the absence of  $\text{HO}_x$  (He et al., 2021b) and  $\text{I}_2\text{O}_2 + \text{O}_3$  reaction was recently found to be the critical step for the  $\text{HIO}_3$  formation (Finkenzeller et al., 2023). The diurnal  
435 patterns show that the maximum of daytime  $\text{HIO}_3$  concentration mimic that of  $\text{O}_3$  in all seasons, indicating that  $\text{O}_3$  may influence terrestrial  $\text{HIO}_3$  formation. However, the role of  $\text{O}_3$  in  $\text{HIO}_3$  formation can be multifaceted and warrants more thorough discussion in the future studies with extensive measurements of other iodine compounds in inland regions, especially urbanized areas. On one hand, chamber studies have shown direct involvement of  $\text{O}_3$  in the formation of  $\text{HIO}_3$  precursors in less  
440 chemically complex scenarios. On the other hand,  $\text{O}_3$  has been proved to simulate the release of iodine compounds in marine environments from surface sea water (Carpenter et al., 2013) and similar processes are likely to occur in urban environments as well. Additionally, temperature may also have favourable impacts on both the formation of  $\text{HIO}_3$  and the release of iodine precursors, which will be discussed in the next section.

445

Moreover, CS in Nanjing shows an opposite profile to T and  $\text{O}_3$ , whereas it keeps almost the same trend as that of Nanjing but fluctuates a little during the day in Beijing spring and winter, which show median values only in 2019. In summary, the diurnal patterns shown in Fig. 2 suggest that stronger solar radiation coupled with higher mixing ratio of  $\text{O}_3$  and higher T are likely the factors favouring the formation of  
450 acids, the low CS at noon is preferred for the survival of acid vapour. Additionally, the diurnal variation of  $\text{HIO}_x$  at BUCT shows stronger seasonality with highest values at around noon in the summer. The maximum concentrations at spring and autumn are similar, while the maximum concentrations in the winter are roughly one order of magnitude lower. At SORPES,  $\text{HIO}_x$  reaches similar levels in the spring, summer and autumn but its concentration is lower in the winter. Consistently, the diurnal maximum  $\text{HIO}_3$   
455 concentration in summer approaches  $10^6 \text{ cm}^{-3}$  at both sites.



### 3.2.3 Iodine sources

In order to investigate the source of  $\text{HIO}_x$  in urban environments, we further conduct cluster analysis of the air mass backward trajectories of the AHL/BUCT station in warm seasons (from May to September in this study). The  $\text{HIO}_3$  precursor proxy calculated from Eq. (13) based on the measurement results at BUCT/AHL station is classified into four levels as shown in Fig. S5 (see Supplement S4 for more details). High precursor levels are mainly associated with air masses originating from the south and southeast, whereas lower iodine precursor concentrations are associated with northern air masses. It implies that marine iodine sources could be important for the AHL/BUCT station due to long range transport. Additionally, the air mass travels from northern wind may also carry substantial precursors of  $\text{HIO}_3$ , indicating the potential terrestrial sources of iodine. Therefore, both marine (O'Dowd and Hoffmann, 2005; Carpenter et al., 2021) and terrestrial precursors such as soil fumigants (Li et al., 2014; Wang et al., 2017) may contribute to the  $\text{HIO}_3$  formation at the AHL/BUCT site.

Both seasonal variation and diurnal pattern shows the lowest concentration of  $\text{HIO}_x$  in winter when the impact from residential coal burning and fossil fuel combustion power plant in Beijing is the largest. It implies that  $\text{HIO}_x$  concentration is not promoted by pollution in cold season. The negative correlation between  $\text{HIO}_3$  and BC shown in Fig. S6 further demonstrate the irrelevance of winter pollution on the  $\text{HIO}_3$  in Beijing. A previous 2-year measurements conducted in Beijing show that high loadings of particulate organic iodine compounds (OICs) occurred in the heating season, and HOI was thought to be the key oxidant to form the OICs (Shi et al., 2021). The different seasonal distribution between gaseous  $\text{HIO}_x$  in this study and particle-phase OICs indicates potentially different iodine sources of gaseous and particulate phases, which warrants further investigation. Fig. 3(a) presents  $\text{HIO}_3$  in different  $\text{PM}_{2.5}$  ranges and shows lower  $\text{HIO}_3$  concentrations when  $\text{PM}_{2.5}$  increases.  $\text{PM}_{2.5}$  measurements in the Beijing–Tianjin–Hebei region (2013 to 2020) show obvious seasonal characteristics with lowest concentrations in summer and highest concentrations in winter (Yang et al., 2022). This phenomenon should be attributed to the inherently independent seasonality of these two constituents instead of any correlation. If the  $\text{PM}_{2.5}$  is a source of gaseous iodine species, the  $\text{HIO}_3$  concentrations should be higher in winter months, which is not the case. Additionally, summertime  $\text{HIO}_3$  concentrations in different  $\text{PM}_{2.5}$  concentration bins have no difference (Fig. 3(b)), which further indicates that the  $\text{HIO}_3$  is not correlated with the particulate matter

pollution in Beijing. Furthermore, the results in Fig. S7 demonstrate that PM<sub>2.5</sub> pollution does not play a conclusive role on the HIO<sub>3</sub> production, especially with the seasonal influence excluded.

There is no definite evidence to justify whether marine or land sources could better explain our  
490 observation on HIO<sub>3</sub> concentration in Beijing. In the marine environments, the rapid reaction of sea-  
surface iodide with O<sub>3</sub> is believed to be the largest global source of iodine species in the forms of  
molecular iodine, I<sub>2</sub> and hypoiodous acid, HOI (Carpenter et al., 2021; Carpenter et al., 2013), which in  
turn contributes to the formation of HIO<sub>x</sub> (Finkenzeller et al., 2023; He et al., 2021b). However, the  
photolysis lifetimes of HOI (~140 s) and I<sub>2</sub> (~10 s), or biogenic volatile iodocarbons (e.g., CH<sub>2</sub>I<sub>2</sub> (~ 5  
495 min)) are too short to contribute to the formation of HIO<sub>x</sub> in Beijing and Nanjing considering the long-  
range transportation (Saiz-Lopez et al., 2012). Another iodine-containing species, methyl iodide (CH<sub>3</sub>I),  
has a longer lifetime of about 5 days which may potentially go through the long-range transportation and  
eventually reach inland cities. CH<sub>3</sub>I is dominantly formed from photochemical processes in the marine  
surface (Moore and Zafiriou, 1994) and additionally also from dust stimulated abiotic emission (Williams  
500 et al., 2007). CH<sub>3</sub>I concentration was shown to be correlated with surface seawater temperature (SST) in  
marine boundary layer air at midlatitude (Yokouchi et al., 2008). Others reported the opposite results in  
the Yellow Sea and the East China Sea during summer (Li et al., 2021) and the reason may be that higher  
surface water temperature also accelerates the chemical loss of CH<sub>3</sub>I from the seawater and atmospheric  
CH<sub>3</sub>I is readily photolyzed. Long-term variations of atmospheric CH<sub>3</sub>I at several sites show that SST  
505 near each site cannot fully explain the variation of observed CH<sub>3</sub>I concentrations (Yokouchi et al., 2012).  
Other factors such as acidification, i.e., pH conditions, mineral dust deposition and dissolved organic  
carbon (DOC) concentration (Li et al., 2021), as well as ferric ion (Fe<sup>3+</sup>) concentration (Chen et al., 2020)  
in seawater could also contribute to the emission rate of CH<sub>3</sub>I.

510 Apart from marine sources, terrestrial sources of CH<sub>3</sub>I including most rice paddies (Redeker et al., 2000),  
terrestrial biomes (Sive et al., 2007), minor wetlands (Dimmer et al., 2001), and biomass burning  
(Andreae et al., 1996) were also proposed. High concentration of CH<sub>3</sub>I at two inland sites in Japan  
indicates the greater importance of terrestrial sources in the summer compared to oceanic sources  
(Yokouchi et al., 2008). As CH<sub>3</sub>I emission from rice paddies is positively correlated with temperature  
515 (Redeker and Cicerone, 2004; Redeker et al., 2000), CH<sub>3</sub>I emission is likely to be stronger in the

summertime. This is consistent with higher concentrations of  $\text{HIO}_x$  in Beijing and Nanjing as shown in Fig. 1, 2 and 4. Moreover, experiments show that  $\text{CH}_3\text{I}$  emission under dark incubation was much lower than that under light incubation and  $\text{CH}_3\text{I}$  production under visible light conditions is lower than that under natural light (Li et al., 2021). Those results indicate that ultraviolet light promotes the production of  $\text{CH}_3\text{I}$  (Chen et al., 2020; Li et al., 2021) as well as its photochemical oxidation. This is consistent with our observation that  $\text{HIO}_x$  is only formed in the daytime (Fig. 4).

The relative importance of terrestrial and marine iodine sources may vary widely with local meteorological factors and the transportation of air masses. Future efforts are needed to verify the composition and distribution of  $\text{HIO}_x$  precursors in polluted environments.

### 3.2.4 Formation of $\text{HIO}_3$ in urban environments

Quantum chemical methods and laboratory experiments have both been carried out to investigate the formation mechanisms of  $\text{HIO}_3$ . Previous studies using quantum chemical calculations have proposed two possible formation pathways of  $\text{HIO}_3$ . Iodine monoxide (IO) was proposed to react with  $\text{HO}_2$  radical to yield  $\text{HIO}_3$  (Drougas and Kosmas, 2005). The reaction between iodine dioxide (OIO) and OH radical was also suggested to produce  $\text{HIO}_3$  (Plane et al., 2006). Laminar flow reactor experiments have also been carried out to investigate the formation mechanisms of  $\text{HIO}_3$  from  $\text{I}_2$  (He, 2017). With the illumination of green-fluorescent lamp,  $\text{I}_2$  was efficiently photolyzed while  $\text{O}_3$  photolysis was restricted, and thus there was no known source of  $\text{HO}_x$ . Surprisingly, a significant amount of  $\text{HIO}_3$  was formed essentially under  $\text{HO}_x$  free conditions. To rule out a potential unknown OH source in the flow reactor, different OH scavengers (methane, sulfur dioxide, cyclohexene and acetic acid) were injected but the production of  $\text{HIO}_3$  remained. Iodine atoms or iodine oxides were proposed to be the reactants with ozone and water to produce  $\text{HIO}_3$ . Following studies from the CLOUD experiments suggest that iodoxy hypiodite (IOIO) could be efficiently converted into  $\text{HIO}_3$  via reactions R (1) and R (2) (Finkenzeller et al., 2023) which successfully explain earlier laboratory and field observations (Sipilä et al., 2016; He et al., 2021b). These results align with our observations at the AHL/BUCT station. UVB is an indication of light intensity and influences the production of I atoms from the photolysis of  $\text{I}_2$  and  $\text{CH}_3\text{I}$ . The produced iodine atoms react with  $\text{O}_3$  and further drive gaseous iodine chemistry (Saiz-Lopez et al., 2012).

545 Fig. 4 depicts the correlation of UVB, O<sub>3</sub> and temperature. Although the correlation between HIO<sub>3</sub> concentration and air temperature is not very strong, high HIO<sub>3</sub> concentrations appear when both the UVB and O<sub>3</sub> mixing ratios are high. This is consistent with the fact that both solar radiation and O<sub>3</sub> are required to initiate the iodine emission and iodine photochemistry.



### 3.3 Iodic acid enhances the particle survival probability

Statistical results show that NPF events occur frequently at both sites throughout the measurement  
555 periods. Whether freshly nucleated particles can contribute to cloud condensation nuclei and hence impose influence on climate and human health depends largely on how fast they grow into larger particles and survive from coagulation scavenging by pre-existing aerosols, which is more efficient for smaller particles. The GR of newly formed particles is therefore central for sub-10 nm particle lifetimes in ambient environment. Earlier studies have linked some dimensionless parameters L or L<sub>Γ</sub> (McMurry et al., 2005; Kuang et al., 2010; Cai et al., 2017b) to justify the occurrence of NPF and described the  
560 competition between aerosol surface area and condensable vapours during the growth period. Recently, a dimensionless survival parameter P (Kulmala et al., 2017) was proposed as the ratio of CS' (CS/10<sup>-4</sup> s<sup>-1</sup>) to GR' (GR/1nm hour<sup>-1</sup>). From this ratio, P shows the competition between the possibility of being cleared and growing to survive. When P is below 50 in clean environment or 100 in polluted urban cities, the SP of the sub-3 nm particles is agreed with the atmospheric observations (Kulmala et al., 2017). As  
565 shown in Fig. S8, the median P is about 50 for the sub-3 nm particles, whereas the median P value is about 20 for 3-7 nm particles in the NPF events at the AHL/BUCT station. That means the growing particles in those days preferred to survive and thus showed us clear new particle formation and further growth.

570

As shown in Eq. (8), the impact of GR on survival of new particles is not linear and a small enhancement on GR could result in much larger enhancement in particle survival probability (Cai et al., 2021a). It also means that the SP of these newly formed particles exhibits a substantial variability, spanning more than

three orders of magnitude, as illustrated in Tables S2~4. To further illustrate the non-linear response of  
575 particle SP, we plot the logarithmic value of SP ( $\log_{10} SP$ ) as a function of CoagS and GR from 1.5 to 3  
nm (Fig. 5(a)) and from 3 to 7 nm (Fig. 5(b)), respectively. The value of SP is extremely sensitive both  
to CoagS and GR. Under the typical CoagS (around  $0.0025 \text{ s}^{-1}$ ) at both sites, the SP could be enhanced  
by more than two orders of magnitude when GR is varied from 1 to  $10 \text{ nm h}^{-1}$ . Increased GR caused by  
additional condensing vapours enables faster growth, which in turn facilitates the survival of sub-10 nm  
580 particles from coagulation scavenging (Kuang et al., 2012). This effect is especially important for sub-3  
nm particles as they are the most susceptible and are easily lost to large pre-existing particles.

We present case studies of several consecutive NPF events at both sites in Fig. 6. At AHL/BUCT station,  
NPF events occurred from May 25 to 29, 2021 due to favourable meteorological conditions, except for  
585 one undefined day (May 27, 2021) when no obvious growth was observed. On this undefined day, the  
UVB in the daytime was low and the intensity was fluctuating, due to cloudiness. Both of these conditions,  
as well as the higher CS, suppressed the NPF (Kerminen et al., 2018; Deng et al., 2020a; Cai et al.,  
2021b). On the other hand, both T and  $\text{O}_3$ , as well as UVB, increased from around 6:00 in the morning  
on the NPF event days, with decreasing RH. The averaged concentrations of  $\text{H}_2\text{SO}_4$  and  $\text{HIO}_3$  in the  
590 particle growth periods from 1.5 nm to 7 nm on event days and from 8:00 to 10:00 on the other days  
were summarized in Table 1. The ratio of  $\text{HIO}_3$  concentration to  $\text{H}_2\text{SO}_4$  was about 5% in the first three  
days and more than 10% in the next two days, likely due to higher  $\text{O}_3$  concentrations which contributes  
to the emission of iodine precursors.

595 Table S2~S4 and S5~S7 summarise the  $\text{HIO}_3$  contribution to GR and SP in the particle size range of 1.5-  
3 nm and 3-7 nm, respectively. To account for the uncertainties in the GR and SP calculations, the  
measured GR are calculated using three methods, namely the APT-x, APT-y and the mode-fitting (MOD)  
methods (see Methods part, Fig. S9). We present the results from MOD methods in the main text to keep  
consistency with earlier studies (Deng et al., 2020b; Qiao et al., 2021). Only events with clear growth  
600 were reported in this study to reduce systematic uncertainties resulting from the GR calculation. We also  
provide the results from the APT-x and APT-y methods in the supplementary materials for completeness.  
The results in Table S2-S4 show that the contributions of  $\text{HIO}_3$  to  $\text{GR}_{<3}$  on May 25 and 26 were lower  
than 5%, whereas the contribution was about 10% on May 29. The  $\text{SP}_{1.5-3}$  enhancement from  $\text{HIO}_3$  is

much stronger on May 29, even reaching 40.5%. Although the contribution of  $\text{HIO}_3$  to  $\text{GR}_{<3}$  on Jun 21, 2021 is almost identical to that on May 29, 2021, SP enhancements on Jun 21, 2021 is 2.5 times larger. This is a result from the 5 times CoagS on Jun 21, 2021. This suggests that in polluted environments with higher CoagS, such as Beijing, SP enhancement can be more sensitive to GR enhancement. Results in both Fig. 7 and Fig. S10 show that the median contribution of  $\text{HIO}_3$  to the GR of particles in the 1.5-3 nm size range is 7.4% using the MOD method, whereas the contribution is only around 3% and 2% using the APT-*x* and APT-*y* methods, respectively. This is resulted from the difference in the measured GR calculated using either the APT or the MOD methods. This further translates into 10.8%, 4.1%, 40.5% SP EF using MOD, APT-*x* and APT-*y* methods, respectively. Despite the uncertainty in the measurement GR calculation, the EF of  $\text{HIO}_3$  to sub-3 nm particle SP is clear: in 33.3%, 25.0% and 55.6% of the events  $\text{HIO}_3$  enhances particle SP by more than 30%, using MOD, APT-*x* and APT-*y* methods, respectively.

Additionally, we show three consecutive NPF events observed from 16 to 18 August 2019 at the SORPES station, Nanjing. These events feature high acid concentrations,  $\text{O}_3$  mixing ratios and strong light intensities as well as low RH and CS. No nucleation mode particles burst was observed on August 20 probably owing to decreased  $\text{H}_2\text{SO}_4$  concentration. Compared to the cases in Beijing, the concentrations of  $\text{O}_3$  and acids are twice as higher at the SORPES station due to geographical and seasonal differences (Table 1).

From June to December 2019, there are 23 NPF events recognized at the SORPES station. Due to the detection limitation of the instruments at SORPES, the sub-3 nm particles were not clearly measured, which in turn poses challenges to get the measured GR through the 50% appearance time method nor the mode fitting method. The statistics are depicted in a different way from that of the AHL/BUCT (see supplementary materials for further details). Briefly, the contribution of  $\text{HIO}_3$  and  $\text{H}_2\text{SO}_4$  to sub-3 nm particle GR in NPF events are quantified based on Eq. (9), Eq. (10) and Eq. (11). This is based on the observed consistency between the gaseous  $\text{H}_2\text{SO}_4$  concentration and its significant contribution to the sub-3 nm particle growth rate in Beijing (Deng et al., 2020b). The SP enhancement is further calculated based on Eq. (12). Consistent with the observation at the AHL/BUCT station, the concentration of gaseous  $\text{HIO}_3$  in Nanjing is lower than  $\text{H}_2\text{SO}_4$  throughout the measurement period, accounting for 10~20% of concentration (Fig. 1(e)). However, the average  $\text{HIO}_3$ : $\text{H}_2\text{SO}_4$  ratio (16.8%) is higher than that in Beijing (10.7%).

The calculated GR contribution of HIO<sub>3</sub> and H<sub>2</sub>SO<sub>4</sub> to sub-3 nm particles (Ratio<sub>1.5-3</sub>) are listed in Table S8, respectively, where the statistical ratios of acid contributions for each NPF event are listed as well.

635 The computations of Eq. (9) and Eq. (10) are subject to acid concentrations and hence the average acid concentrations for individual NPF events dominate the statistics of GR ratio. At the SORPES station from June to November 2019, the contribution of HIO<sub>3</sub> to sub-3 nm particle growth accounts for 6.1% (median) and 6.7% (mean) of H<sub>2</sub>SO<sub>4</sub>.

640 As listed in Table S9, estimated particle survival probability of particles growing from 1.5 to 3 nm considering H<sub>2</sub>SO<sub>4</sub> as the governing contributor (SP<sub>1.5-3</sub>(SA)) is significantly enhanced when counting the contribution from HIO<sub>3</sub> (SP<sub>1.5-3</sub>(SA+IA)). The enhancement of SP with IA being an additional GR contributor varies from 3% to more than 100% in favourable cases, with a median enhancement of 54.3%. For sub-3 nm particles, the survival probability is twice as higher (enhancement factors exceeding 100%)  
645 considering HIO<sub>3</sub> as additional GR contributor on July 3 and October 26. As depicted in Fig. S11(c), SP enhancements in percentage are generally one order of magnitude higher than the GR contribution in percentage and HIO<sub>3</sub> can result in as high as 2-fold enhancement on SP in sub-3 nm particle growth.

The statistical results at both sites suggest that for polluted environments with higher CoagS, GR  
650 enhancement is especially important for the survival of small particles. In Beijing, HIO<sub>3</sub> contributes 7.4% (median) to sub-3 nm particle growth and 2.6% (median) to 3-7 nm particle growth in all NPF events from May to September. Despite the limited GR contribution, it could lead to 40.5% enhancement of SP<sub><3</sub>, whereas there is only a negligible increase of 3.2% (median) for SP<sub>3-7</sub>, estimated using the MOD method. In exceptional cases, we found that HIO<sub>3</sub> could enhance particle SP by more than two-  
655 fold in 22.2% of cases. The median value of GR contribution of HIO<sub>3</sub> accounts for 6.1% of H<sub>2</sub>SO<sub>4</sub> and the median enhancement of 1.5-3 nm particles survival probability reaches 47.6% when consider HIO<sub>3</sub> as an additional GR contributor, at the SORPES station in summer 2019. In favourable cases, the gaseous HIO<sub>3</sub> can contribute to more than 14.0% of particle growth, leading to the survival probability of fresh particles enhanced by a factor of two. The role of the other iodine oxoacid, HIO<sub>2</sub>, in particle growth  
660 remains unclear due to the absence of contribution equation like Eq. (10) for HIO<sub>3</sub>. The estimated contribution of HIO<sub>2</sub> derived from the same equation should be significantly smaller compared with that

of  $\text{HIO}_3$  even if the arrival rate of  $\text{HIO}_2$  also reaches the kinetic limit, as measured  $\text{HIO}_2$  concentrations at both sites are much lower than  $\text{HIO}_3$ .

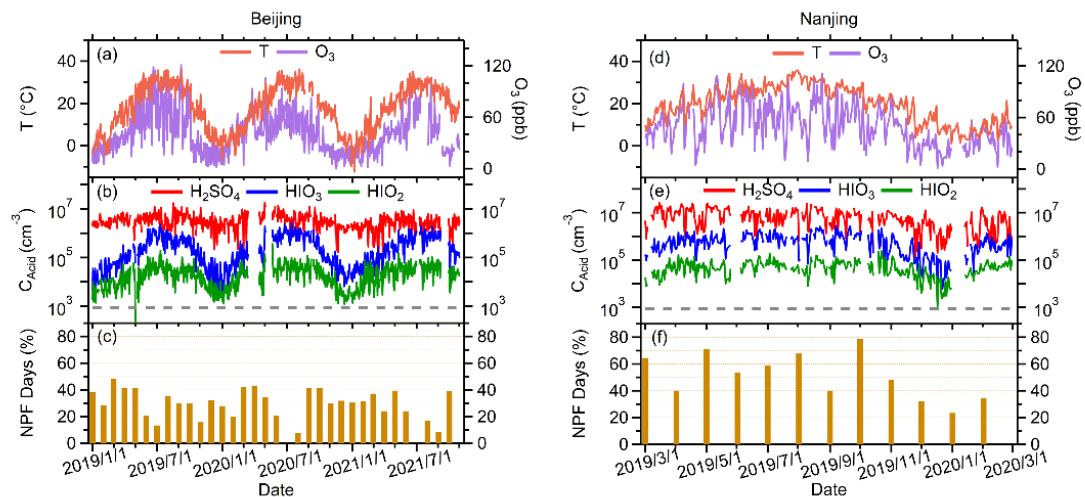
In summary, our findings show that  $\text{HIO}_3$  is an important contributor to sub-3 nm particle survival in these two Chinese cities and similar environments elsewhere in warm seasons. However, for particles in 665 3-7 nm, the contribution of  $\text{HIO}_3$  to particle GR and SP is negligible.

#### 4 Conclusion

In this study, we show three years' measurements of iodine oxoacids ( $\text{HIO}_x$ ) in Beijing and one-year observation in Nanjing. Unlike  $\text{H}_2\text{SO}_4$ ,  $\text{HIO}_3$  has a more prominent seasonal variation at both sites with 670 highest concentrations in summer and lowest concentrations in winter. The diurnal pattern of  $\text{HIO}_x$  indicates that  $\text{HIO}_3$  formation is influenced by photochemical activities and  $\text{O}_3$  concentrations which may together influence the emission of iodine species and the further oxidation chemistry. In Beijing, back trajectory analysis suggests that marine iodine sources are important for the  $\text{HIO}_x$  production and less  $\text{HIO}_x$  is observed if the air masses originate from the North. The lowest concentrations of  $\text{HIO}_x$  in winter 675 and its weak correlation with  $\text{PM}_{2.5}$  implies that anthropogenic activities are likely not the important sources of  $\text{HIO}_x$ .

We find that the median contribution of iodic acid,  $\text{HIO}_3$ , to  $\text{GR}_{\text{sub-3}}$  is less than 10% in Beijing and in Nanjing from May to September. However,  $\text{HIO}_3$  can significantly enhance particle survival probability, 680 occasionally by two-fold, for 1.5-3 nm particles at both sites. This means that although  $\text{H}_2\text{SO}_4$  is considered to be the main driver of sub-3 nm growth in polluted urban areas, additional sources, such as  $\text{HIO}_3$ , needs to be considered. As the growth rate of  $\text{HIO}_3$  is measured to be identical to that of  $\text{H}_2\text{SO}_4$  on a per-molecule basis (He et al., 2021b), we propose that  $\text{HIO}_3$  and  $\text{H}_2\text{SO}_4$  can be summed up when estimating the sub-3 nm particle growth rates. Beside the enhancement on particle growth, recent 685 theoretical studies have indicated that dimethyl amine could potentially accelerate pure  $\text{HIO}_3$  nucleation (Ning et al., 2022). However, experimental confirmation is needed to confirm such prediction and our long-term observation can therefore provide basis for guiding experimental works to use ambient relevant level acid concentrations.

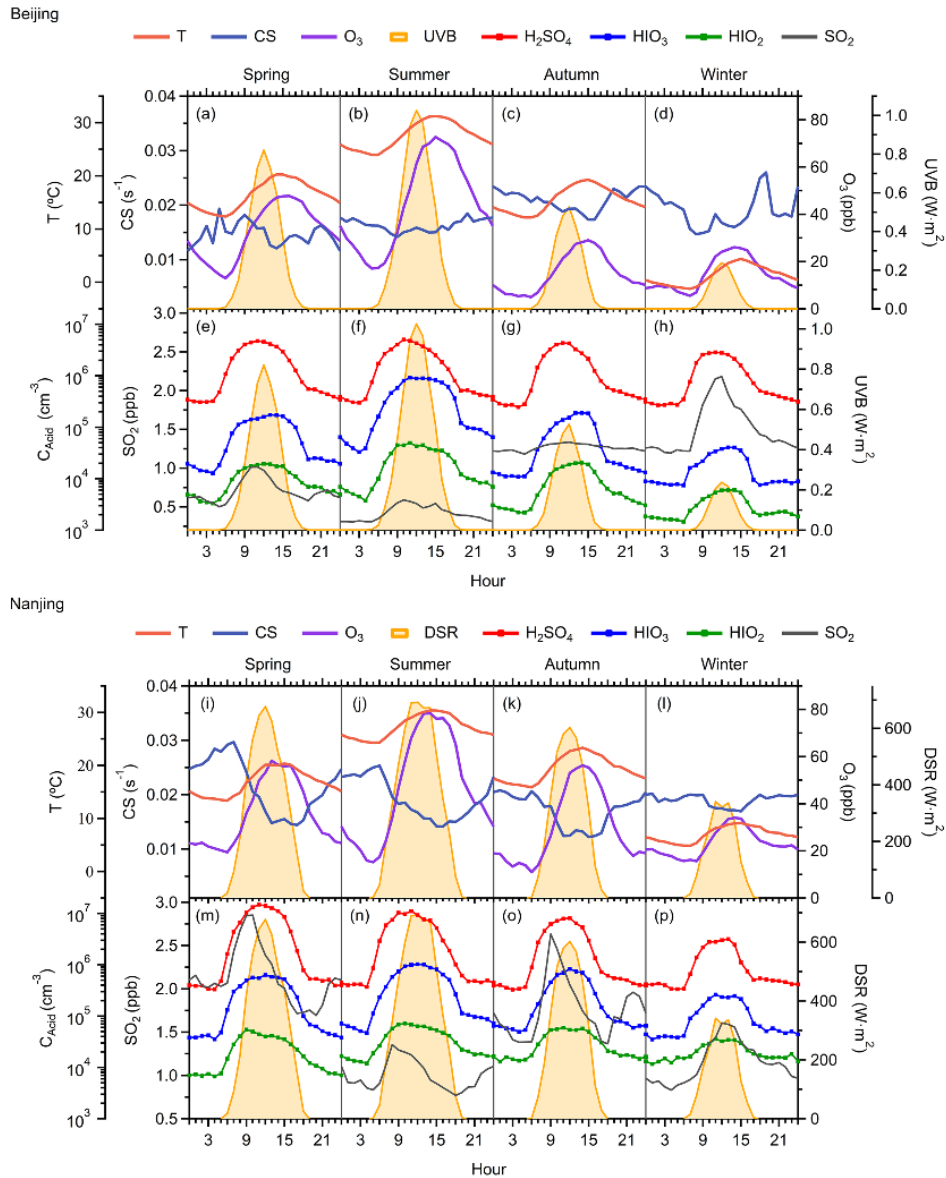




690

**Figure 1.** Timeseries of parameters from Jan 1, 2019 to Oct 31, 2021 in Beijing (a-c) and from March 1, 2019 to Feb 29, 2020 in Nanjing (d-f). (a/d). Temperature and ozone; (b/e). Sulfuric acid and iodine oxoacid concentrations. The grey dashed line represents the detection limit of instruments ( $875 \text{ cm}^{-3}$ ); (c/f). The frequencies of new particle formation events in each month. Time resolution for all the presented data is 1 day and the environmental parameters and vapour concentrations are averaged daytime (8 am to 4 pm) mean.

695



700 **Figure 2.** Diurnal variation of median value of  $O_3$ ,  $T$ , and  $CS$  in the first row (Beijing, a-d) and third row (Nanjing, i-j) and the diurnal variation of median  $SO_2$ ,  $H_2SO_4$  and  $HIO_x$  concentrations in the second row (Beijing, e-h) and fourth row (Nanjing, m-p) in four seasons. The first to last columns are profiles in spring, summer, autumn, and winter, respectively. The diurnal patterns of UVB were plotted in every panel to compare with other factors better.

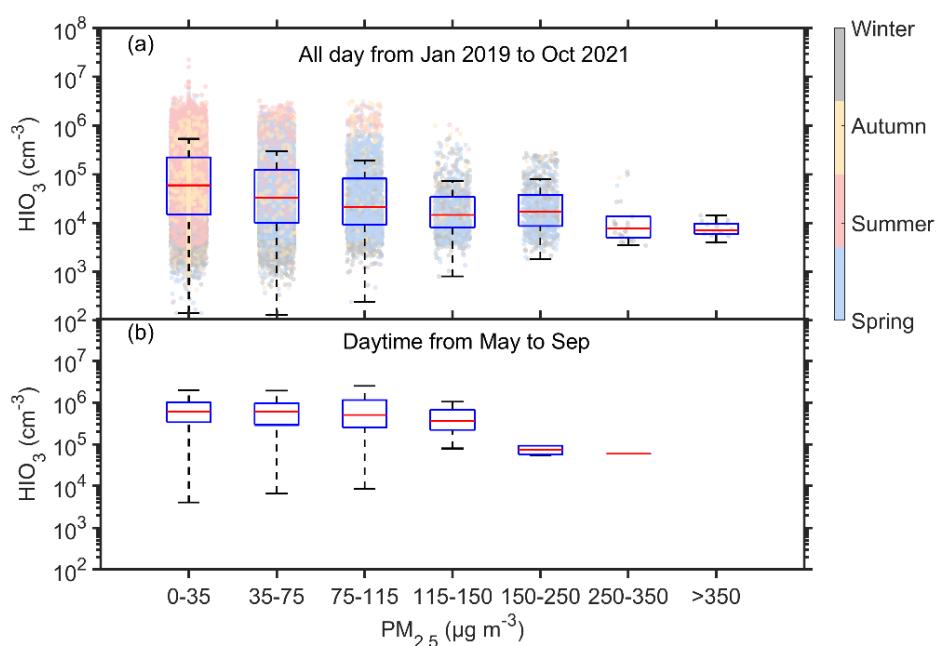
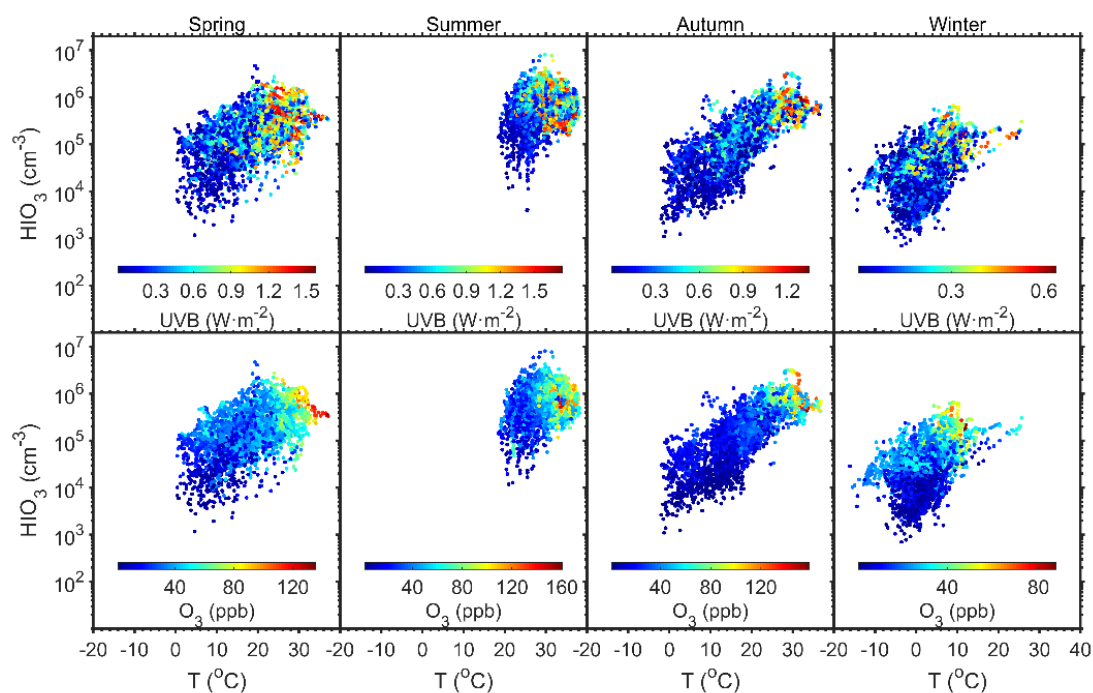


**Figure 3.** HIO<sub>3</sub> concentration in different PM<sub>2.5</sub> level bins. (a) data from the whole campaign coloured by the seasons in Beijing and (b) data in the daytime from May to September (warm seasons) in Beijing.



705

**Figure 4.** Influences of T, UVB, and O<sub>3</sub> on HIO<sub>3</sub> concentration in the daytime (8:00-16:00) in Beijing. The analysis is separated into four seasons.

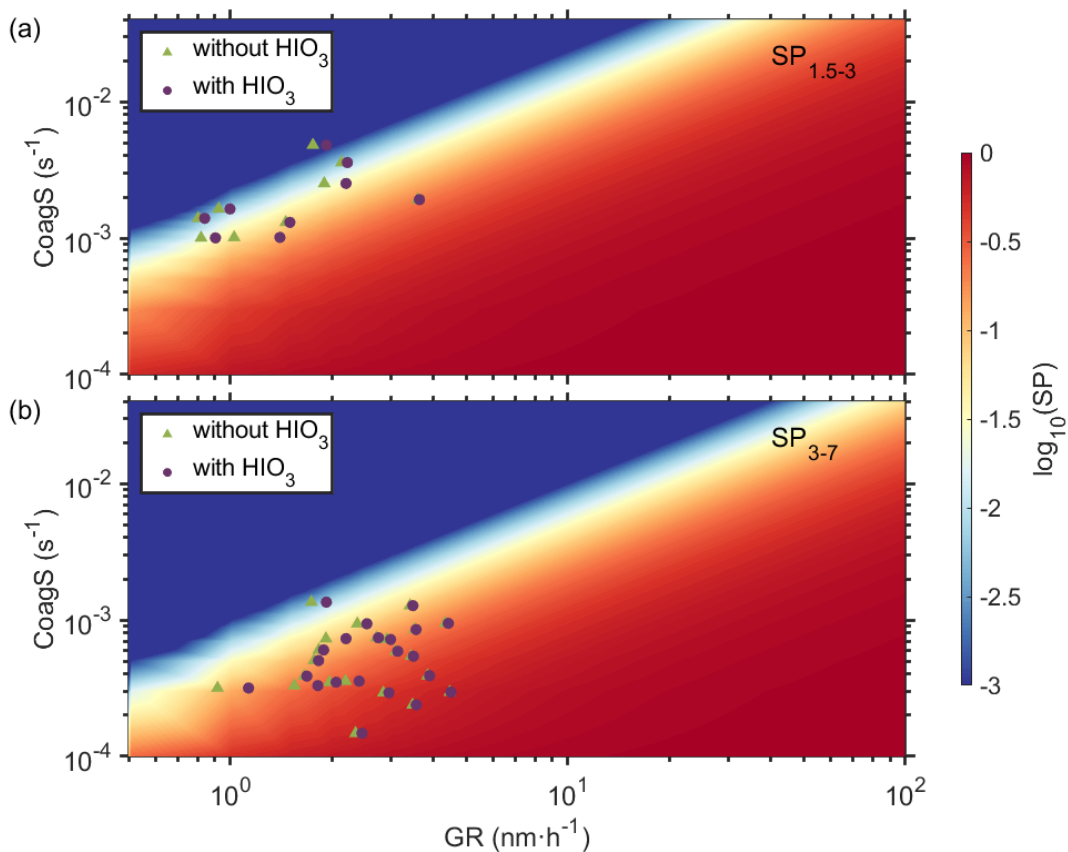


Figure 5. The effect of coagulation sink and growth rate on particle survival probability for 1.5-3 nm (a) and 3-7 nm (b) particles, respectively.

710

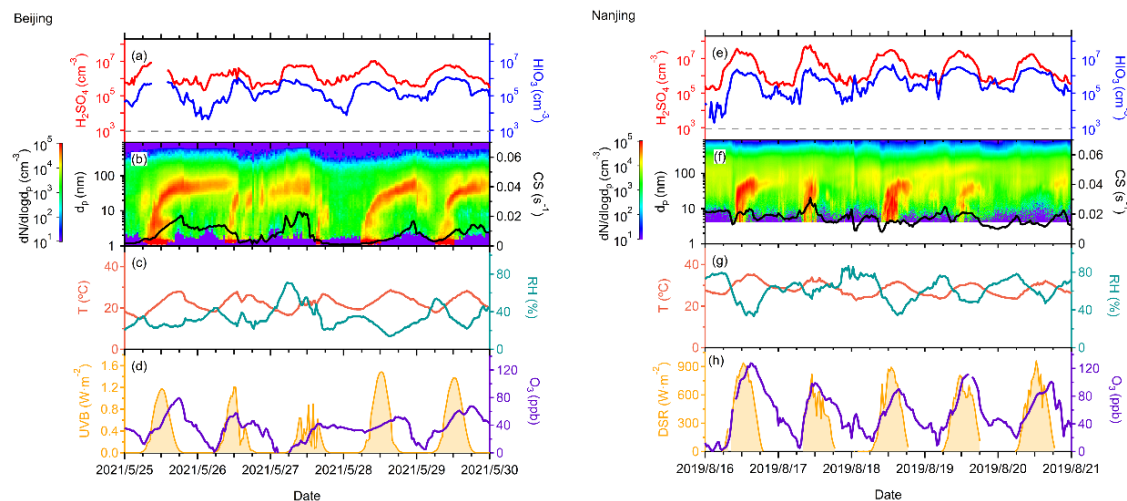
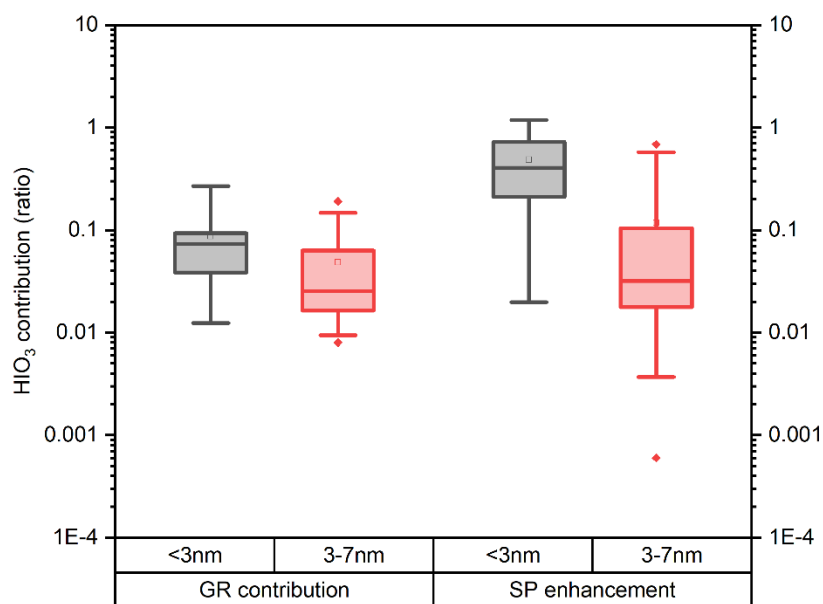


Figure 6. Cases of consecutive NPF events in Beijing (a-d) and Nanjing (e-h) sites. Acid concentrations are shown in the first row, particle number size distribution, and CS are shown in the second row, meteorological factors, such as T, RH, UVB, and O<sub>3</sub> concentrations are also presented in the third and fourth rows. The measurement of acids in the Beijing site was unavailable for a short period on May 25 (panel (a)).

715



**Figure 7.** The contributions in ratio of HIO<sub>3</sub> to growth rate (a) and survival probability enhancement (b) of particles within sub-3nm and 3-7nm in NPF events in the Beijing site utilizing the mode fitting method.

720

**Table 1.** Environmental factors and acid concentrations shown in Figure 5.

Site	Date	Start time	End time	H <sub>2</sub> SO <sub>4</sub> (cm <sup>-3</sup> )	HIO <sub>3</sub> (cm <sup>-3</sup> )	CS (s <sup>-1</sup> )	T (°C)	RH (%)	UVB/DSR (W/m <sup>2</sup> )	O <sub>3</sub> (ppb)
Beijing	2021/5/25	6:50:00	9:23:00	3.96E+06	2.03E+05	0.0046	18.5	26	0.20	25.68
	2021/5/26	9:20:00	10:48:36	8.01E+06	4.90E+05	0.0105	24.25	32	0.84	47.82
	2021/5/27	8:00:00	10:00:00	1.66E+06	5.41E+04	0.0222	19.6	59	0.45	11.17
	2021/5/28	6:00:00	8:15:00	5.35E+06	7.21E+05	0.0018	20.35	34	0.10	31.51
	2021/5/29	6:20:00	9:38:44	3.89E+06	4.99E+05	0.0040	19.4	50	0.25	31.24
Nanjing	2019/8/16	10:22:21	14:59:49	2.03E+07	1.40E+06	0.0200	33.23	40.69	858	105.38
	2019/8/17	8:04:22	11:10:40	4.27E+07	1.79E+06	0.0268	32.02	56.43	525	75.27
	2019/8/18	10:17:53	17:18:42	2.06E+07	2.20E+06	0.0134	30.93	39.52	705.1	81.09
	2019/8/19	8:00:00	10:00:00	1.35E+07	2.48E+06	0.0164	27.99	61.71	419.7	58.72
	2019/8/20	8:00:00	10:00:00	1.07E+07	2.12E+06	0.0154	27.4	67.08	458	48.26

725

*Data availability.* Measurement data at the AHL/BUCT and SORPES station, including acids concentration data, trace gas and aerosol data and meteorological data, are available upon request from the corresponding authors before the relevant databases are open to the public.

730

*Author contributions.* WN and XCH designed the research. YZ, CD, YG, YL, CH, TL and ZW conducted the measurements at the AHL/BUCT station. DL, YL, CL, LC, YL, LW and XC conducted the measurements at the SORPES station. YZ, DL, XCH, WN, CD, RC, YL, YG, TP, FB, XQ, PP, YL, CY, JJ, AD and MK analyzed the data and interpreted the results. YZ, DL, XCH and WN prepared the manuscript with contributions from all co-authors.

735

*Competing interests.* The authors have no competing interests to declare. At least one of the (co-)authors is a member of the editorial board of Atmospheric Chemistry and Physics.

740 *Acknowledgements.* We thank colleagues and students at the AHL/BUCT station and the SORPES station for their contributions to the maintenance of the measurements.

Financial support. This work was supported by the National Natural Science Foundation of China (NSFC) project (92044301, 42220104006, 42075101 and 41975154), the Jiangsu Provincial Collaborative Innovation Center of Climate Change and the Fundamental Research Funds for the Central Universities. Financial support from Samsung PM2.5 SRP is also acknowledged.

745

## Reference:

- Almeida, J., Schobesberger, S., Kürten, A., Ortega, I. K., Kupiainen-Määttä, O., Praplan, A. P., Adamov, A., Amorim, A., Bianchi, F., Breitenlechner, M., David, A., Dommen, J., Donahue, N. M., Downard, A., Dunne, E., Duplissy, J., Ehrhart, S., Flagan, R. C., Franchin, A., Guida, R., Hakala, J., Hansel, A., Heinritzi, M., Henschel, H., Jokinen, T., Junninen, H., Kajos, M., Kangasluoma, J., Keskinen, H., Kupc, A., Kurtén, T., Kvashin, A. N., Laaksonen, A., Lehtipalo, K., Leiminger, M., Leppä, J., Loukonen, V., Makhmutov, V., Mathot, S., McGrath, M. J., Nieminen, T., Olenius, T., Onnela, A., Petäjä, T., Riccobono, F., Riipinen, I., Rissanen, M., Rondo, L., Ruuskanen, T., Santos, F. D., Sarnela, N., Schallhart, S., Schnitzhofer, R., Seinfeld, J. H., Simon, M., Sipilä, M., Stozhkov, Y., Stratmann, F., Tomé, A., Tröstl, J., Tsagkogeorgas, G., Vaattovaara, P., Viisanen, Y., Virtanen, A., Vrtala, A., Wagner, P. E., Weingartner, E., Wex, H., Williamson, C., Wimmer, D., Ye, P., Yli-Juuti, T., Carslaw, K. S., Kulmala, M., Curtius, J., Baltensperger, U., Worsnop, D. R., Vehkamäki, H., and Kirkby, J.: Molecular understanding of sulphuric acid–amine particle nucleation in the atmosphere, *Nature*, 502, 359-363, 10.1038/nature12663, 2013.
- Andreae, M. O., Atlas, E., Harris, G. W., Helas, G., de Kock, A., Koppmann, R., Maenhaut, W., Manø, S., Pollock, W. H., Rudolph, J., Scharffe, D., Schebeske, G., and Welling, M.: Methyl halide emissions from savanna fires in southern Africa, *Journal of Geophysical Research: Atmospheres*, 101, 23603-23613, 10.1029/95jd01733, 1996.
- Baccarini, A., Karlsson, L., Dommen, J., Duplessis, P., Vullers, J., Brooks, I. M., Saiz-Lopez, A., Salter, M., Tjernstrom, M., Baltensperger, U., Zieger, P., and Schmale, J.: Frequent new particle formation over the high Arctic pack ice by enhanced iodine emissions, *Nature Communications*, 11, 4924, 10.1038/s41467-020-18551-0, 2020.
- Beck, L. J., Sarnela, N., Junninen, H., Hoppe, C. J. M., Garmash, O., Bianchi, F., Riva, M., Rose, C., Peräkylä, O., Wimmer, D., Kausiala, O., Jokinen, T., Ahonen, L., Mikkilä, J., Hakala, J., He, X. C., Kontkanen, J., Wolf, K. K. E., Cappelletti, D., Mazzola, M., Traversi, R., Petroselli, C., Viola, A. P., Vitale, V., Lange, R., Massling, A., Nøjgaard, J. K., Krejci, R., Karlsson, L., Zieger, P., Jang, S., Lee, K., Vakkari, V., Lampilahti, J., Thakur, R. C., Leino, K., Kangasluoma, J., Duplissy, E. M., Siivola, E., Marbouti, M., Tham, Y. J., Saiz-Lopez, A., Petäjä, T., Ehn, M., Worsnop, D. R., Skov, H., Kulmala, M., Kerminen, V. M., and Sipilä, M.: Differing Mechanisms of New Particle Formation at Two Arctic Sites, *GRL*, 48, 10.1029/2020gl091334, 2021.
- Bousiotis, D., Brean, J., Pope, F. D., Dall'Osto, M., Querol, X., Alastuey, A., Perez, N., Petäjä, T., Massling, A., Nøjgaard, J. K., Nordstrøm, C., Kouvarakis, G., Vratolis, S., Eleftheriadis, K., Niemi, J. V., Portin, H., Wiedensohler, A., Weinhold, K., Merkel, M., Tuch, T., and Harrison, R. M.: The effect of meteorological conditions and atmospheric composition in the occurrence and development of new particle formation (NPF) events in Europe, *ACP*, 21, 3345-3370, 10.5194/acp-21-3345-2021, 2021.
- Cai, M., Liang, B., Sun, Q., Liu, L., Yuan, B., Shao, M., Huang, S., Peng, Y., Wang, Z., Tan, H., Li, F., Xu, H., Chen, D., and Zhao, J.: The important roles of surface tension and growth rate in the contribution of new particle formation (NPF) to cloud condensation nuclei (CCN) number concentration: evidence from field measurements in southern China, *ACP*, 21, 8575-8592, 10.5194/acp-21-8575-2021, 2021a.
- Cai, R., Chen, D.-R., Hao, J., and Jiang, J.: A miniature cylindrical differential mobility analyzer for sub-3 nm particle sizing, *Journal of Aerosol Science*, 106, 111-119, 10.1016/j.jaerosci.2017.01.004, 2017a.
- Cai, R., Häkkinen, E., Yan, C., Jiang, J., Kulmala, M., and Kangasluoma, J.: The effectiveness of the coagulation sink of 3–10 nm atmospheric particles, *ACP*, 22, 11529-11541, 10.5194/acp-22-11529-2022, 2022a.

- Cai, R., Yang, D., Fu, Y., Wang, X., Li, X., Ma, Y., Hao, J., Zheng, J., and Jiang, J.: Aerosol surface area concentration: a governing factor in new particle formation in Beijing, *ACP*, 17, 12327-12340, 10.5194/acp-17-12327-2017, 2017b.
- 795 Cai, R., Yan, C., Worsnop, D. R., Bianchi, F., Kerminen, V.-M., Liu, Y., Wang, L., Zheng, J., Kulmala, M., and Jiang, J.: An indicator for sulfuric acid–amine nucleation in atmospheric environments, *Aerosol Science and Technology*, 55, 1059-1069, 10.1080/02786826.2021.1922598, 2021b.
- Cai, R., Li, C., He, X.-C., Deng, C., Lu, Y., Yin, R., Yan, C., Wang, L., Jiang, J., Kulmala, M., and Kangasluoma, J.: Impacts of coagulation on the appearance time method for new particle growth rate evaluation and their corrections, *ACP*, 21, 2287-2304, 10.5194/acp-21-2287-2021, 2021c.
- 800 Cai, R., Yan, C., Yang, D., Yin, R., Lu, Y., Deng, C., Fu, Y., Ruan, J., Li, X., Kontkanen, J., Zhang, Q., Kangasluoma, J., Ma, Y., Hao, J., Worsnop, D. R., Bianchi, F., Paasonen, P., Kerminen, V.-M., Liu, Y., Wang, L., Zheng, J., Kulmala, M., and Jiang, J.: Sulfuric acid–amine nucleation in urban Beijing, *ACP*, 21, 2457-2468, 10.5194/acp-21-2457-2021, 2021d.
- Cai, R., Yin, R., Yan, C., Yang, D., Deng, C., Dada, L., Kangasluoma, J., Kontkanen, J., Halonen, R., 805 Ma, Y., Zhang, X., Paasonen, P., Petäjä, T., Kerminen, V. M., Liu, Y., Bianchi, F., Zheng, J., Wang, L., Hao, J., Smith, J. N., Donahue, N. M., Kulmala, M., Worsnop, D. R., and Jiang, J.: The missing base molecules in atmospheric acid-base nucleation, *Natl Sci Rev*, 9, nwac137, 10.1093/nsr/nwac137, 2022b.
- Carpenter, L. J., MacDonald, S. M., Shaw, M. D., Kumar, R., Saunders, R. W., Parthipan, R., Wilson, J., and Plane, J. M. C.: Atmospheric iodine levels influenced by sea surface emissions of inorganic iodine, 810 *Nature Geoscience*, 6, 108-111, 10.1038/ngeo1687, 2013.
- Carpenter, L. J., Chance, R. J., Sherwen, T., Adams, T. J., Ball, S. M., Evans, M. J., Hepach, H., Hollis, L. D. J., Hughes, C., Jickells, T. D., Mahajan, A., Stevens, D. P., Tinel, L., and Wadley, M. R.: Marine iodine emissions in a changing world, *Proceedings of the Royal Society A: Mathematical, Physical and Engineering Sciences*, 477, 10.1098/rspa.2020.0824, 2021.
- 815 Chen, R., Hu, B., Liu, Y., Xu, J., Yang, G., Xu, D., and Chen, C.: Beyond PM<sub>2.5</sub>: The role of ultrafine particles on adverse health effects of air pollution, *Biochimica et Biophysica Acta (BBA) - General Subjects*, 1860, 2844-2855, 10.1016/j.bbagen.2016.03.019, 2016.
- Chen, Y., Liu, S., Yang, G., and He, Z.: Influence Factors on Photochemical Production of Methyl Iodide in Seawater, *Journal of Ocean University of China*, 19, 1353-1361, 10.1007/s11802-020-4463-8, 2020.
- 820 Chu, B., Kerminen, V. M., Bianchi, F., Yan, C., Petäjä, T., and Kulmala, M.: Atmospheric new particle formation in China, *Atmos. Chem. Phys.*, 19, 115-138, 10.5194/acp-19-115-2019, 2019.
- Claudio Tomasi, S. F., and Alexander Kokhanovsky: *Atmospheric Aerosols: Life Cycles and Effects on Air Quality and Climate*, 1-86 pp.2017.
- Cohen, M. D., Stunder, B. J. B., Rolph, G. D., Draxler, R. R., Stein, A. F., and Ngan, F.: NOAA's 825 HYSPLIT Atmospheric Transport and Dispersion Modeling System, *Bulletin of the American Meteorological Society*, 96, 2059-2077, 10.1175/bams-d-14-00110.1, 2015.
- Dada, L., Lehtipalo, K., Kontkanen, J., Nieminen, T., Baalbaki, R., Ahonen, L., Duplissy, J., Yan, C., Chu, B., Petäjä, T., Lehtinen, K., Kerminen, V.-M., Kulmala, M., and Kangasluoma, J.: Formation and growth of sub-3-nm aerosol particles in experimental chambers, *Nature Protocols*, 15, 1013-1040, 830 10.1038/s41596-019-0274-z, 2020.
- Deng, C., Cai, R., Yan, C., Zheng, J., and Jiang, J.: Formation and growth of sub-3 nm particles in megacities: impact of background aerosols, *Faraday Discuss*, 226, 348-363, 10.1039/d0fd00083c, 2020a.
- Deng, C., Fu, Y., Dada, L., Yan, C., Cai, R., Yang, D., Zhou, Y., Yin, R., Lu, Y., Li, X., Qiao, X., Fan, X., Nie, W., Kontkanen, J., Kangasluoma, J., Chu, B., Ding, A., Kerminen, V. M., Paasonen, P., Worsnop,



- 835 D. R., Bianchi, F., Liu, Y., Zheng, J., Wang, L., Kulmala, M., and Jiang, J.: Seasonal Characteristics of New Particle Formation and Growth in Urban Beijing, *EST*, 54, 8547-8557, 10.1021/acs.est.0c00808, 2020b.
- Dimmer, C. H., Simmonds, P. G., Nickless, G., and Bassford, M. R. J. A. E.: Biogenic fluxes of halomethanes from Irish peatland ecosystems, *Atmospheric Environment*, 35, 321-330, Doi 840 10.1016/S1352-2310(00)00151-5, 2001.
- Ding, A., Nie, W., Huang, X., Chi, X., Sun, J., Kerminen, V.-M., Xu, Z., Guo, W., Petäjä, T., Yang, X., Kulmala, M., and Fu, C.: Long-term observation of air pollution-weather/climate interactions at the SORPES station: a review and outlook, *Frontiers of Environmental Science & Engineering*, 10, 15, 10.1007/s11783-016-0877-3, 2016.
- 845 Ding, A., Huang, X., Nie, W., Chi, X., Xu, Z., Zheng, L., Xu, Z., Xie, Y., Qi, X., Shen, Y., Sun, P., Wang, J., Wang, L., Sun, J., Yang, X.-Q., Qin, W., Zhang, X., Cheng, W., Liu, W., Pan, L., and Fu, C.: Significant reduction of PM<sub>2.5</sub> in eastern China due to regional-scale emission control: evidence from SORPES in 2011–2018, *ACP*, 19, 11791-11801, 10.5194/acp-19-11791-2019, 2019.
- Downward, G. S., van Nunen, E., Kerckhoffs, J., Vineis, P., Brunekreef, B., Boer, J. M. A., Messier, K. 850 P., Roy, A., Verschuren, W. M. M., van der Schouw, Y. T., Sluijs, I., Gulliver, J., Hoek, G., and Vermeulen, R.: Long-Term Exposure to Ultrafine Particles and Incidence of Cardiovascular and Cerebrovascular Disease in a Prospective Study of a Dutch Cohort, *Environmental Health Perspectives*, 126, 127007, 10.1289/EHP3047, 2018.
- Drougas, E. and Kosmas, A. M. J. T. J. o. P. C. A.: Computational studies of (HIO<sub>3</sub>) isomers and the 855 HO<sub>2</sub>+ IO reaction pathways, 109, 3887-3892, 2005.
- Ehn, M., Thornton, J. A., Kleist, E., Sipilä, M., Junninen, H., Pullinen, I., Springer, M., Rubach, F., Tillmann, R., Lee, B., Lopez-Hilfiker, F., Andres, S., Acir, I.-H., Rissanen, M., Jokinen, T., Schobesberger, S., Kangasluoma, J., Kontkanen, J., Nieminen, T., Kurtén, T., Nielsen, L. B., Jørgensen, S., Kjaergaard, H. G., Canagaratna, M., Maso, M. D., Berndt, T., Petäjä, T., Wahner, A., Kerminen, V.- 860 M., Kulmala, M., Worsnop, D. R., Wildt, J., and Mentel, T. F.: A large source of low-volatility secondary organic aerosol, *Nature*, 506, 476-479, 10.1038/nature13032, 2014.
- Finkenzeller, H., Iyer, S., He, X.-C., Simon, M., Koenig, T. K., Lee, C. F., Valiev, R., Hofbauer, V., Amorim, A., Baalbaki, R., Baccarini, A., Beck, L., Bell, D. M., Caudillo, L., Chen, D., Chiu, R., Chu, B., Dada, L., Duplissy, J., Heinritzi, M., Kempainen, D., Kim, C., Krechmer, J., Kürten, A., Kvashnin, 865 A., Lamkaddam, H., Lee, C. P., Lehtipalo, K., Li, Z., Makhmutov, V., Manninen, H. E., Marie, G., Marten, R., Mauldin, R. L., Mentler, B., Müller, T., Petäjä, T., Philippov, M., Ranjithkumar, A., Rörup, B., Shen, J., Stolzenburg, D., Tauber, C., Tham, Y. J., Tomé, A., Vazquez-Pufleau, M., Wagner, A. C., Wang, D. S., Wang, M., Wang, Y., Weber, S. K., Nie, W., Wu, Y., Xiao, M., Ye, Q., Zauner-Wieczorek, M., Hansel, A., Baltensperger, U., Brioude, J., Curtius, J., Donahue, N. M., Haddad, I. E., Flagan, R. C., 870 Kulmala, M., Kirkby, J., Sipilä, M., Worsnop, D. R., Kurten, T., Rissanen, M., and Volkamer, R.: The gas-phase formation mechanism of iodic acid as an atmospheric aerosol source, *Nature Chemistry*, 15, 129-135, 10.1038/s41557-022-01067-z, 2023.
- Fuks, N. A. and Sutugin, A. G.: *Highly Dispersed Aerosols*, Ann Arbor Science Publishers 1970.
- Gomez Martin, J. C., Lewis, T. R., Blitz, M. A., Plane, J. M. C., Kumar, M., Francisco, J. S., and Saiz- 875 Lopez, A.: A gas-to-particle conversion mechanism helps to explain atmospheric particle formation through clustering of iodine oxides, *Nature Communications*, 11, 4521, 10.1038/s41467-020-18252-8, 2020.

- Guo, Y., Yan, C., Li, C., Ma, W., Feng, Z., Zhou, Y., Lin, Z., Dada, L., Stolzenburg, D., Yin, R., Kontkanen, J., Daellenbach, K. R., Kangasluoma, J., Yao, L., Chu, B., Wang, Y., Cai, R., Bianchi, F., Liu, Y., and Kulmala, M.: Formation of nighttime sulfuric acid from the ozonolysis of alkenes in Beijing, *ACP*, 21, 5499-5511, 10.5194/acp-21-5499-2021, 2021.
- 880 He, X.-C., Iyer, S., Sipilä, M., Ylisirniö, A., Peltola, M., Kontkanen, J., Baalbaki, R., Simon, M., Kürten, A., Tham, Y. J., Pesonen, J., Ahonen, L. R., Amanatidis, S., Amorim, A., Baccharini, A., Beck, L., Bianchi, F., Brilke, S., Chen, D., Chiu, R., Curtius, J., Dada, L., Dias, A., Dommen, J., Donahue, N. M., Duplissy, J., El Haddad, I., Finkenzeller, H., Fischer, L., Heinritzi, M., Hofbauer, V., Kangasluoma, J., Kim, C., Koenig, T. K., Kubečka, J., Kvashnin, A., Lamkaddam, H., Lee, C. P., Leiminger, M., Li, Z., Makhmutov, V., Xiao, M., Marten, R., Nie, W., Onnela, A., Partoll, E., Petäjä, T., Salo, V.-T., Schuchmann, S., Steiner, G., Stolzenburg, D., Stozhkov, Y., Tauber, C., Tomé, A., Väisänen, O., Vazquez-Pufleau, M., Volkamer, R., Wagner, A. C., Wang, M., Wang, Y., Wimmer, D., Winkler, P. M., Worsnop, D. R., Wu, Y., Yan, C., Ye, Q., Lehtinen, K., Nieminen, T., Manninen, H. E., Rissanen, M., Schobesberger, S., Lehtipalo, K., Baltensperger, U., Hansel, A., Kerminen, V.-M., Flagan, R. C., Kirkby, J., Kurtén, T., and Kulmala, M.: Determination of the collision rate coefficient between charged iodic acid clusters and iodic acid using the appearance time method, *Aerosol Science and Technology*, 55, 231-242, 10.1080/02786826.2020.1839013, 2021a.
- 885 He, X.-C., Tham, Y. J., Dada, L., Wang, M., Finkenzeller, H., Stolzenburg, D., Iyer, S., Simon, M., Kürten, A., Shen, J., Rörup, B., Rissanen, M., Schobesberger, S., Baalbaki, R., Wang, D. S., Koenig, T. K., Jokinen, T., Sarnela, N., Beck, L. J., Almeida, J., Amanatidis, S., Amorim, A., Ataei, F., Baccharini, A., Bertozzi, B., Bianchi, F., Brilke, S., Caudillo, L., Chen, D., Chiu, R., Chu, B., Dias, A., Ding, A., Dommen, J., Duplissy, J., El Haddad, I., Gonzalez Carracedo, L., Granzin, M., Hansel, A., Heinritzi, M., Hofbauer, V., Junninen, H., Kangasluoma, J., Kempainen, D., Kim, C., Kong, W., Krechmer, J. E., Kvashin, A., Laitinen, T., Lamkaddam, H., Lee, C. P., Lehtipalo, K., Leiminger, M., Li, Z., Makhmutov, V., Manninen, H. E., Marie, G., Marten, R., Mathot, S., Mauldin, R. L., Mentler, B., Möhler, O., Müller, T., Nie, W., Onnela, A., Petäjä, T., Pfeifer, J., Philippov, M., Ranjithkumar, A., Saiz-Lopez, A., Salma, I., Scholz, W., Schuchmann, S., Schulze, B., Steiner, G., Stozhkov, Y., Tauber, C., Tomé, A., Thakur, R. C., Väisänen, O., Vazquez-Pufleau, M., Wagner, A. C., Wang, Y., Weber, S. K., Winkler, P. M., Wu, Y., Xiao, M., Yan, C., Ye, Q., Ylisirniö, A., Zauner-Wieczorek, M., Zha, Q., Zhou, P., Flagan, R. C., Curtius, J., Baltensperger, U., Kulmala, M., Kerminen, V.-M., Kurtén, T., Donahue, N. M., Volkamer, R., Kirkby, J., Worsnop, D. R., and Sipilä, M.: Role of iodine oxoacids in atmospheric aerosol nucleation, *Science*, 371, 589-595, 10.1126/science.abe0298, 2021b.
- 900 He, X.: From the measurement of halogenated species to iodine particle formation, 2017.
- 910 He, X. C., Shen, J., Iyer, S., Juuti, P., Zhang, J., Koirala, M., Kytökari, M. M., Worsnop, D. R., Rissanen, M., Kulmala, M., Maier, N. M., Mikkilä, J., Sipilä, M., and Kangasluoma, J.: Characterisation of gaseous iodine species detection using the multi-scheme chemical ionisation inlet 2 with bromide and nitrate chemical ionisation methods, *Atmos. Meas. Tech.*, 16, 4461-4487, 10.5194/amt-16-4461-2023, 2023.
- Hoffmann, T., O'Dowd, C. D., and Seinfeld, J. H.: Iodine oxide homogeneous nucleation: An explanation for coastal new particle production, *GRL*, 28, 1949-1952, 10.1029/2000gl012399, 2001.
- Jiang, J., Chen, M., Kuang, C., Attoui, M., and McMurry, P. H.: Electrical Mobility Spectrometer Using a Diethylene Glycol Condensation Particle Counter for Measurement of Aerosol Size Distributions Down to 1 nm, *Aerosol Science and Technology*, 45, 510-521, 10.1080/02786826.2010.547538, 2011.

- 920 Jiang, S., Zhang, F., Ren, J., Chen, L., Yan, X., Liu, J., Sun, Y., and Li, Z.: Evaluation of the contribution of new particle formation to cloud droplet number concentration in the urban atmosphere, *ACP*, 21, 14293-14308, 10.5194/acp-21-14293-2021, 2021.
- Jimenez, J. L.: New particle formation from photooxidation of diiodomethane (CH<sub>2</sub>I<sub>2</sub>), *Journal of Geophysical Research*, 108, 10.1029/2002jd002452, 2003.
- 925 Jokinen, T., Lehtipalo, K., Thakur, R. C., Ylivinkka, I., Neitola, K., Sarnela, N., Laitinen, T., Kulmala, M., Petäjä, T., and Sipilä, M.: Measurement report: Long-term measurements of aerosol precursor concentrations in the Finnish subarctic boreal forest, *ACP*, 22, 2237-2254, 10.5194/acp-22-2237-2022, 2022.
- Jokinen, T., Sipilä, M., Junninen, H., Ehn, M., Lönn, G., Hakala, J., Petäjä, T., Mauldin, R. L., Kulmala, M., and Worsnop, D. R.: Atmospheric sulphuric acid and neutral cluster measurements using CI-API-TOF, *ACP*, 12, 4117-4125, 10.5194/acp-12-4117-2012, 2012.
- 930 Jokinen, T., Sipilä, M., Kontkanen, J., Vakkari, V., Tisler, P., Duplissy, E.-M., Junninen, H., Kangasluoma, J., Manninen, H., and Petäjä, T. J. S. A.: Ion-induced sulfuric acid–ammonia nucleation drives particle formation in coastal Antarctica, *Science Advances*, 4, eaat9744, 2018.
- 935 Junninen, H., Ehn, M., Petäjä, T., Luosujärvi, L., Kotiaho, T., Kostianen, R., Rohner, U., Gonin, M., Fuhrer, K., Kulmala, M., and Worsnop, D. R.: A high-resolution mass spectrometer to measure atmospheric ion composition, *Atmospheric Measurement Techniques*, 3, 1039-1053, 10.5194/amt-3-1039-2010, 2010.
- Kalkavouras, P., Bougiatioti, A., Kalivitis, N., Stavroulas, I., Tombrou, M., Nenes, A., and Mihalopoulos, N.: Regional new particle formation as modulators of cloud condensation nuclei and cloud droplet number in the eastern Mediterranean, *ACP*, 19, 6185-6203, 10.5194/acp-19-6185-2019, 2019.
- 940 Kalkavouras, P., Bossioli, E., Bezantakos, S., Bougiatioti, A., Kalivitis, N., Stavroulas, I., Kouvarakis, G., Protonotariou, A. P., Dandou, A., Biskos, G., Mihalopoulos, N., Nenes, A., and Tombrou, M.: New particle formation in the southern Aegean Sea during the Etesians: importance for CCN production and cloud droplet number, *ACP*, 17, 175-192, 10.5194/acp-17-175-2017, 2017.
- 945 Kerminen, V.-M., Lihavainen, H., Komppula, M., Viisanen, Y., and Kulmala, M.: Direct observational evidence linking atmospheric aerosol formation and cloud droplet activation, *GRL*, 32, 10.1029/2005gl023130, 2005.
- Kerminen, V.-M., Chen, X., Vakkari, V., Petäjä, T., Kulmala, M., and Bianchi, F.: Atmospheric new particle formation and growth: review of field observations, *ERL*, 13, 10.1088/1748-9326/aadf3c, 2018.
- 950 Kirkby, J., Curtius, J., Almeida, J., Dunne, E., Duplissy, J., Ehrhart, S., Franchin, A., Gagné, S., Ickes, L., Kürten, A., Kupc, A., Metzger, A., Riccobono, F., Rondo, L., Schobesberger, S., Tsagkogeorgas, G., Wimmer, D., Amorim, A., Bianchi, F., Breitenlechner, M., David, A., Dommen, J., Downard, A., Ehn, M., Flagan, R. C., Haider, S., Hansel, A., Hauser, D., Jud, W., Junninen, H., Kreissl, F., Kvashin, A., Laaksonen, A., Lehtipalo, K., Lima, J., Lovejoy, E. R., Makhmutov, V., Mathot, S., Mikkilä, J., Minginette, P., Mogo, S., Nieminen, T., Onnela, A., Pereira, P., Petäjä, T., Schnitzhofer, R., Seinfeld, J. H., Sipilä, M., Stozhkov, Y., Stratmann, F., Tomé, A., Vanhanen, J., Viisanen, Y., Vrtala, A., Wagner, P. E., Walther, H., Weingartner, E., Wex, H., Winkler, P. M., Carslaw, K. S., Worsnop, D. R., Baltensperger, U., and Kulmala, M.: Role of sulphuric acid, ammonia and galactic cosmic rays in atmospheric aerosol nucleation, *Nature*, 476, 429-433, 10.1038/nature10343, 2011.
- 960 Kirkby, J., Duplissy, J., Sengupta, K., Frege, C., Gordon, H., Williamson, C., Heinritzi, M., Simon, M., Yan, C., Almeida, J., Tröstl, J., Nieminen, T., Ortega, I. K., Wagner, R., Adamov, A., Amorim, A., Bernhammer, A.-K., Bianchi, F., Breitenlechner, M., Brilke, S., Chen, X., Craven, J., Dias, A., Ehrhart,

S., Flagan, R. C., Franchin, A., Fuchs, C., Guida, R., Hakala, J., Hoyle, C. R., Jokinen, T., Junninen, H.,  
965 Kangasluoma, J., Kim, J., Krapf, M., Kürten, A., Laaksonen, A., Lehtipalo, K., Makhmutov, V., Mathot,  
S., Molteni, U., Onnela, A., Peräkylä, O., Piel, F., Petäjä, T., Praplan, A. P., Pringle, K., Rap, A., Richards,  
N. A. D., Riipinen, I., Rissanen, M. P., Rondo, L., Sarnela, N., Schobesberger, S., Scott, C. E., Seinfeld,  
J. H., Sipilä, M., Steiner, G., Stozhkov, Y., Stratmann, F., Tomé, A., Virtanen, A., Vogel, A. L., Wagner,  
A. C., Wagner, P. E., Weingartner, E., Wimmer, D., Winkler, P. M., Ye, P., Zhang, X., Hansel, A.,  
970 Dommen, J., Donahue, N. M., Worsnop, D. R., Baltensperger, U., Kulmala, M., Carslaw, K. S., and  
Curtius, J.: Ion-induced nucleation of pure biogenic particles, *Nature*, 533, 521-526,  
10.1038/nature17953, 2016.

Kuang, C., Chen, M., Zhao, J., Smith, J., McMurry, P. H., and Wang, J.: Size and time-resolved growth  
rate measurements of 1 to 5 nm freshly formed atmospheric nuclei, *ACP*, 12, 3573-3589, 10.5194/acp-  
975 12-3573-2012, 2012.

Kuang, C., Riipinen, I., Sihto, S. L., Kulmala, M., McCormick, A. V., and McMurry, P. H.: An improved  
criterion for new particle formation in diverse atmospheric environments, *ACP*, 10, 8469-8480,  
10.5194/acp-10-8469-2010, 2010.

Kulmala, M., Kerminen, V. M., Anttila, T., Laaksonen, A., and O'Dowd, C. D.: Organic aerosol  
980 formation via sulphate cluster activation, *Journal of Geophysical Research: Atmospheres*, 109, Artn  
D0420510.1029/2003jd003961, 2004a.

Kulmala, M., Kerminen, V. M., Petaja, T., Ding, A. J., and Wang, L.: Atmospheric gas-to-particle  
conversion: why NPF events are observed in megacities?, *Faraday Discuss*, 200, 271-288,  
10.1039/c6fd00257a, 2017.

985 Kulmala, M., Vehkamäki, H., Petäjä, T., Dal Maso, M., Lauri, A., Kerminen, V. M., Birmili, W., and  
McMurry, P. H.: Formation and growth rates of ultrafine atmospheric particles: a review of observations,  
*Journal of Aerosol Science*, 35, 143-176, 10.1016/j.jaerosci.2003.10.003, 2004b.

Kulmala, M., Maso, M. D., Mäkelä, J., Pirjola, L., Väkevä, M., Aalto, P., Miikkulainen, P., Hämeri, K.,  
and O'Dowd, C. J. T. B.: On the formation, growth and composition of nucleation mode particles, 53,  
990 479-490, 2001.

Kulmala, M., Cai, R., Stolzenburg, D., Zhou, Y., Dada, L., Guo, Y., Yan, C., Petäjä, T., Jiang, J., and  
Kerminen, V. M.: The contribution of new particle formation and subsequent growth to haze formation,  
*Environ Sci Atmos*, 2, 352-361, 10.1039/d1ea00096a, 2022.

Kulmala, M., Petäjä, T., Nieminen, T., Sipilä, M., Manninen, H. E., Lehtipalo, K., Dal Maso, M., Aalto,  
995 P. P., Junninen, H., Paasonen, P., Riipinen, I., Lehtinen, K. E. J., Laaksonen, A., and Kerminen, V.-M.:  
Measurement of the nucleation of atmospheric aerosol particles, *Nature Protocols*, 7, 1651-1667,  
10.1038/nprot.2012.091, 2012.

Kulmala, M., Dada, L., Daellenbach, K. R., Yan, C., Stolzenburg, D., Kontkanen, J., Ezhova, E., Hakala,  
S., Tuovinen, S., Kokkonen, T. V., Kurppa, M., Cai, R., Zhou, Y., Yin, R., Baalbaki, R., Chan, T., Chu,  
1000 B., Deng, C., Fu, Y., Ge, M., He, H., Heikkinen, L., Junninen, H., Liu, Y., Lu, Y., Nie, W., Rusanen, A.,  
Vakkari, V., Wang, Y., Yang, G., Yao, L., Zheng, J., Kujansuu, J., Kangasluoma, J., Petaja, T., Paasonen,  
P., Jarvi, L., Worsnop, D., Ding, A., Liu, Y., Wang, L., Jiang, J., Bianchi, F., and Kerminen, V. M.: Is  
reducing new particle formation a plausible solution to mitigate particulate air pollution in Beijing and  
other Chinese megacities?, *Faraday Discuss*, 226, 334-347, 10.1039/d0fd00078g, 2021.

1005 Kurten, A., Rondo, L., Ehrhart, S., and Curtius, J.: Calibration of a Chemical Ionization Mass  
Spectrometer for the Measurement of Gaseous Sulfuric Acid, *Journal of Physical Chemistry A*, 116,  
6375-6386, 10.1021/jp212123n, 2012.

- Kürten, A., Bergen, A., Heinritzi, M., Leiminger, M., Lorenz, V., Piel, F., Simon, M., Sitals, R., Wagner, A. C., and Curtius, J.: Observation of new particle formation and measurement of sulfuric acid, ammonia, amines and highly oxidized organic molecules at a rural site in central Germany, *ACP*, 16, 12793-12813, 10.5194/acp-16-12793-2016, 2016.
- 1010 Laakso, L., Petaja, T., Lehtinen, K. E. J., Kulmala, M., Paatero, J., Horrak, U., Tammet, H., and Joutsensaari, J.: Ion production rate in a boreal forest based on ion, particle and radiation measurements, *ACP*, 4, 1933-1943, DOI 10.5194/acp-4-1933-2004, 2004.
- 1015 Lehtinen, K., Korhonen, H., Maso, M. D., and Kulmala, M. J. B. E. R.: On the concept of condensation sink diameter, 8, 405-411, 2003.
- Lehtinen, K. E. J., Dal Maso, M., Kulmala, M., and Kerminen, V.-M.: Estimating nucleation rates from apparent particle formation rates and vice versa: Revised formulation of the Kerminen–Kulmala equation, *Journal of Aerosol Science*, 38, 988-994, 10.1016/j.jaerosci.2007.06.009, 2007.
- 1020 Lehtipalo, K., Kontkanen, J., Kangasluoma, J., Franchin, A., and Research, J. L. J. B. E.: Methods for determining particle size distribution and growth rates between 1 and 3 nm using the Particle Size Magnifier, 19, 215-236, 2014.
- Lehtipalo, K., Yan, C., Dada, L., Bianchi, F., Xiao, M., Wagner, R., Stolzenburg, D., Ahonen, L. R., Amorim, A., Baccarini, A., Bauer, P. S., Baumgartner, B., Bergen, A., Bernhammer, A. K., Breitenlechner, M., Brilke, S., Buchholz, A., Mazon, S. B., Chen, D., Chen, X., Dias, A., Dommen, J., Draper, D. C., Duplissy, J., Ehn, M., Finkenzeller, H., Fischer, L., Frege, C., Fuchs, C., Garmash, O., Gordon, H., Hakala, J., He, X., Heikkinen, L., Heinritzi, M., Helm, J. C., Hofbauer, V., Hoyle, C. R., Jokinen, T., Kangasluoma, J., Kerminen, V. M., Kim, C., Kirkby, J., Kontkanen, J., Kürten, A., Lawler, M. J., Mai, H., Mathot, S., Mauldin, R. L., 3rd, Molteni, U., Nichman, L., Nie, W., Nieminen, T., Ojdanic, A., Onnela, A., Passananti, M., Petäjä, T., Piel, F., Pospisilova, V., Quéléver, L. L. J., Rissanen, M. P., Rose, C., Sarnela, N., Schallhart, S., Schuchmann, S., Sengupta, K., Simon, M., Sipilä, M., Tauber, C., Tomé, A., Tröstl, J., Väisänen, O., Vogel, A. L., Volkamer, R., Wagner, A. C., Wang, M., Weitz, L., Wimmer, D., Ye, P., Ylisirniö, A., Zha, Q., Carslaw, K. S., Curtius, J., Donahue, N. M., Flagan, R. C., Hansel, A., Riipinen, I., Virtanen, A., Winkler, P. M., Baltensperger, U., Kulmala, M., and Worsnop, D.
- 1030 R.: Multicomponent new particle formation from sulfuric acid, ammonia, and biogenic vapors, *Sci Adv*, 4, eaau5363, 10.1126/sciadv.aau5363, 2018.
- Li, H., Ning, A., Zhong, J., Zhang, H., Liu, L., Zhang, Y., Zhang, X., Zeng, X. C., and He, H.: Influence of atmospheric conditions on sulfuric acid-dimethylamine-ammonia-based new particle formation, *Chemosphere*, 245, 125554, 10.1016/j.chemosphere.2019.125554, 2020.
- 1040 Li, Y., He, Z., Yang, G. P., and Zou, Y.: Spatial distribution and biogeochemical cycling of methyl iodide in the Yellow Sea and the East China Sea during summer, *Environmental Pollution*, 276, 116749, 10.1016/j.envpol.2021.116749, 2021.
- Li, Y., Chi, L., Mao, L., Yan, D., Wu, Z., Ma, T., Guo, M., Wang, Q., Ouyang, C., and Cao, A.: Control of Soilborne Pathogens of *Zingiber officinale* by Methyl Iodide and Chloropicrin in China, *Plant Dis*, 98, 384-388, 10.1094/PDIS-06-13-0623-RE, 2014.
- 1045 Liu, J., Jiang, J., Zhang, Q., Deng, J., and Hao, J.: A spectrometer for measuring particle size distributions in the range of 3 nm to 10  $\mu$ m, *Frontiers of Environmental Science & Engineering*, 10, 63-72, 10.1007/s11783-014-0754-x, 2016.
- Liu, Y., Nie, W., Li, Y., Ge, D., Liu, C., Xu, Z., Chen, L., Wang, T., Wang, L., Sun, P., Qi, X., Wang, J., Xu, Z., Yuan, J., Yan, C., Zhang, Y., Huang, D., Wang, Z., Donahue, N. M., Worsnop, D., Chi, X., Ehn, M., and Ding, A.: Formation of condensable organic vapors from anthropogenic and biogenic volatile
- 1050

- organic compounds (VOCs) is strongly perturbed by NO<sub>x</sub> in eastern China, *Atmos. Chem. Phys.*, 21, 14789-14814, 10.5194/acp-21-14789-2021, 2021.
- 1055 Liu, Y., Yan, C., Feng, Z., Zheng, F., Fan, X., Zhang, Y., Li, C., Zhou, Y., Lin, Z., Guo, Y., Zhang, Y., Ma, L., Zhou, W., Liu, Z., Dada, L., Dällenbach, K., Kontkanen, J., Cai, R., Chan, T., Chu, B., Du, W., Yao, L., Wang, Y., Cai, J., Kangasluoma, J., Kokkonen, T., Kujansuu, J., Rusanen, A., Deng, C., Fu, Y., Yin, R., Li, X., Lu, Y., Liu, Y., Lian, C., Yang, D., Wang, W., Ge, M., Wang, Y., Worsnop, D. R., Junninen, H., He, H., Kerminen, V.-M., Zheng, J., Wang, L., Jiang, J., Petäjä, T., Bianchi, F., and Kulmala, M.: Continuous and comprehensive atmospheric observations in Beijing: a station to understand the complex urban atmospheric environment, *Big Earth Data*, 4, 295-321, 10.1080/20964471.2020.1798707, 2020.
- 1060 Lu, Y., Yan, C., Fu, Y., Chen, Y., Liu, Y., Yang, G., Wang, Y., Bianchi, F., Chu, B., Zhou, Y., Yin, R., Baalbaki, R., Garmash, O., Deng, C., Wang, W., Liu, Y., Petäjä, T., Kerminen, V.-M., Jiang, J., Kulmala, M., and Wang, L.: A proxy for atmospheric daytime gaseous sulfuric acid concentration in urban Beijing, *ACP*, 19, 1971-1983, 10.5194/acp-19-1971-2019, 2019.
- 1065 Mahfouz, N. G. A. and Donahue, N. M.: Technical note: The enhancement limit of coagulation scavenging of small charged particles, *ACP*, 21, 3827-3832, 10.5194/acp-21-3827-2021, 2021.
- Mäkelä, J. M.: Biogenic iodine emissions and identification of end-products in coastal ultrafine particles during nucleation bursts, *Journal of Geophysical Research*, 107, 10.1029/2001jd000580, 2002.
- 1070 Manninen, H. E., Mirme, S., Mirme, A., Petäjä, T., and Kulmala, M.: How to reliably detect molecular clusters and nucleation mode particles with Neutral cluster and Air Ion Spectrometer (NAIS), *Atmospheric Measurement Techniques*, 9, 3577-3605, 10.5194/amt-9-3577-2016, 2016.
- McMurry, P. H., Fink, M., Sakurai, H., Stolzenburg, M. R., Mauldin, R. L., Smith, J., Eisele, F., Moore, K., Sjostedt, S., Tanner, D., Huey, L. G., Nowak, J. B., Edgerton, E., and Voisin, D.: A criterion for new particle formation in the sulfur-rich Atlanta atmosphere, *Journal of Geophysical Research*, 110, 10.1029/2005jd005901, 2005.
- 1075 Moore, R. M. and Zafiriou, O. C.: Photochemical Production of Methyl-Iodide in Seawater, *J Geophys Res-Atmos*, 99, 16415-16420, Doi 10.1029/94jd00786, 1994.
- Nie, W., Yan, C., Huang, D. D., Wang, Z., Liu, Y., Qiao, X., Guo, Y., Tian, L., Zheng, P., Xu, Z., Li, Y., Xu, Z., Qi, X., Sun, P., Wang, J., Zheng, F., Li, X., Yin, R., Dallenbach, K. R., Bianchi, F., Petäjä, T., Zhang, Y., Wang, M., Schervish, M., Wang, S., Qiao, L., Wang, Q., Zhou, M., Wang, H., Yu, C., Yao, D., Guo, H., Ye, P., Lee, S., Li, Y. J., Liu, Y., Chi, X., Kerminen, V.-M., Ehn, M., Donahue, N. M., Wang, T., Huang, C., Kulmala, M., Worsnop, D., Jiang, J., and Ding, A.: Secondary organic aerosol formed by condensing anthropogenic vapours over China's megacities, *Nature Geoscience*, 15, 255-261, 10.1038/s41561-022-00922-5, 2022.
- 1085 Nieminen, T., Lehtinen, K. E. J., and Kulmala, M.: Sub-10 nm particle growth by vapor condensation – effects of vapor molecule size and particle thermal speed, *ACP*, 10, 9773-9779, 10.5194/acp-10-9773-2010, 2010.
- Ning, A., Liu, L., Zhang, S., Yu, F., Du, L., Ge, M., and Zhang, X.: The critical role of dimethylamine in the rapid formation of iodine acid particles in marine areas, *npj Climate and Atmospheric Science*, 5, 92, 10.1038/s41612-022-00316-9, 2022.
- 1090 O'Dowd, C. D. and Hoffmann, T.: Coastal New Particle Formation: A Review of the Current State-Of-The-Art, *Environmental Chemistry*, 2, 10.1071/en05077, 2005.

- O'Dowd, C. D., Jimenez, J. L., Bahreini, R., Flagan, R. C., Seinfeld, J. H., Hämeri, K., Pirjola, L.,  
 1095 Kulmala, M., Jennings, S. G., and Hoffmann, T.: Marine aerosol formation from biogenic iodine  
 emissions, *Nature*, 417, 632-636, 10.1038/nature00775, 2002.
- Paasonen, P., Peltola, M., Kontkanen, J., Junninen, H., Kerminen, V.-M., and Kulmala, M.:  
 Comprehensive analysis of particle growth rates from nucleation mode to cloud condensation nuclei in  
 boreal forest, *ACP*, 18, 12085-12103, 10.5194/acp-18-12085-2018, 2018.
- 1100 Paasonen, P., Asmi, A., Petäjä, T., Kajos, M. K., Äijälä, M., Junninen, H., Holst, T., Abbatt, J. P. D.,  
 Arneth, A., Birmili, W., van der Gon, H. D., Hamed, A., Hoffer, A., Laakso, L., Laaksonen, A., Richard  
 Leaitch, W., Plass-Dülmer, C., Pryor, S. C., Räisänen, P., Swietlicki, E., Wiedensohler, A., Worsnop, D.  
 R., Kerminen, V.-M., and Kulmala, M.: Warming-induced increase in aerosol number concentration  
 likely to moderate climate change, *Nature Geoscience*, 6, 438-442, 10.1038/ngeo1800, 2013.
- 1105 Petäjä, T., Mauldin, I. R. L., Kosciuch, E., McGrath, J., Nieminen, T., Paasonen, P., Boy, M., Adamov,  
 A., Kotiaho, T., and Kulmala, M.: Sulfuric acid and OH concentrations in a boreal forest site, *Atmos.  
 Chem. Phys.*, 9, 7435-7448, 10.5194/acp-9-7435-2009, 2009.
- Plane, J., Joseph, D., Allan, B., Ashworth, S., and Francisco, J. J. T. J. o. P. C. A.: An experimental and  
 theoretical study of the reactions  $\text{OIO} + \text{NO}$  and  $\text{OIO} + \text{OH}$ , 110, 93-100, 2006.
- 1110 Qi, X. M., Ding, A. J., Nie, W., Petäjä, T., Kerminen, V. M., Herrmann, E., Xie, Y. N., Zheng, L. F.,  
 Manninen, H., Aalto, P., Sun, J. N., Xu, Z. N., Chi, X. G., Huang, X., Boy, M., Virkkula, A., Yang, X.  
 Q., Fu, C. B., and Kulmala, M.: Aerosol size distribution and new particle formation in the western  
 Yangtze River Delta of China: 2 years of measurements at the SORPES station, *ACP*, 15, 12445-12464,  
 10.5194/acp-15-12445-2015, 2015.
- 1115 Qiao, X., Yan, C., Li, X., Guo, Y., Yin, R., Deng, C., Li, C., Nie, W., Wang, M., Cai, R., Huang, D.,  
 Wang, Z., Yao, L., Worsnop, D. R., Bianchi, F., Liu, Y., Donahue, N. M., Kulmala, M., and Jiang, J.:  
 Contribution of Atmospheric Oxygenated Organic Compounds to Particle Growth in an Urban  
 Environment, *EST*, 55, 13646-13656, 10.1021/acs.est.1c02095, 2021.
- Redeker, K. R. and Cicerone, R. J.: Environmental controls over methyl halide emissions from rice  
 1120 paddies, *Global Biogeochemical Cycles*, 18, 10.1029/2003gb002092, 2004.
- Redeker, K. R., Wang, N., Low, J. C., McMillan, A., Tyler, S. C., and Cicerone, R. J.: Emissions of  
 methyl halides and methane from rice paddies, *Science*, 290, 966-969, 10.1126/science.290.5493.966,  
 2000.
- Saiz-Lopez, A., Plane, J. M., Baker, A. R., Carpenter, L. J., von Glasow, R., Martin, J. C., McFiggans,  
 1125 G., and Saunders, R. W.: Atmospheric chemistry of iodine, *Chemical Reviews*, 112, 1773-1804,  
 10.1021/cr200029u, 2012.
- Shi, X., Qiu, X., Chen, Q., Chen, S., Hu, M., Rudich, Y., and Zhu, T.: Organic Iodine Compounds in  
 Fine Particulate Matter from a Continental Urban Region: Insights into Secondary Formation in the  
 Atmosphere, *EST*, 55, 1508-1514, 10.1021/acs.est.0c06703, 2021.
- 1130 Sipilä, M., Sarnela, N., Jokinen, T., Henschel, H., Junninen, H., Kontkanen, J., Richters, S., Kangasluoma,  
 J., Franchin, A., Peräkylä, O., Rissanen, M. P., Ehn, M., Vehkamäki, H., Kurten, T., Berndt, T., Petäjä,  
 T., Worsnop, D., Ceburnis, D., Kerminen, V.-M., Kulmala, M., and O'Dowd, C.: Molecular-scale  
 evidence of aerosol particle formation via sequential addition of  $\text{HIO}_3$ , *Nature*, 537, 532-534,  
 10.1038/nature19314, 2016.
- 1135 Sive, B. C., Varner, R. K., Mao, H., Blake, D. R., Wingenter, O. W., and Talbot, R.: A large terrestrial  
 source of methyl iodide, *GRL*, 34, 10.1029/2007gl030528, 2007.

- Stolzenburg, D., Cai, R., Blichner, S. M., Kontkanen, J., Zhou, P., Makkonen, R., Kerminen, V.-M., Kulmala, M., Riipinen, I., and Kangasluoma, J.: Atmospheric nanoparticle growth, *Reviews of Modern Physics*, 95, 045002, 10.1103/RevModPhys.95.045002, 2023.
- 1140 Stolzenburg, D., Simon, M., Ranjithkumar, A., Kürten, A., Lehtipalo, K., Gordon, H., Ehrhart, S., Finkenzeller, H., Pichelstorfer, L., Nieminen, T., He, X.-C., Brilke, S., Xiao, M., Amorim, A., Baalbaki, R., Baccarini, A., Beck, L., Bräkling, S., Caudillo Murillo, L., Chen, D., Chu, B., Dada, L., Dias, A., Dommen, J., Duplissy, J., El Haddad, I., Fischer, L., Gonzalez Carracedo, L., Heinritzi, M., Kim, C., Koenig, T. K., Kong, W., Lamkaddam, H., Lee, C. P., Leiminger, M., Li, Z., Makhmutov, V., Manninen, H. E., Marie, G., Marten, R., Müller, T., Nie, W., Partoll, E., Petäjä, T., Pfeifer, J., Philippov, M., Rissanen, M. P., Rörup, B., Schobesberger, S., Schuchmann, S., Shen, J., Sipilä, M., Steiner, G., Stozhkov, Y., Tauber, C., Tham, Y. J., Tomé, A., Vazquez-Pufleau, M., Wagner, A. C., Wang, M., Wang, Y., Weber, S. K., Wimmer, D., Wlasits, P. J., Wu, Y., Ye, Q., Zauner-Wieczorek, M., Baltensperger, U., Carslaw, K. S., Curtius, J., Donahue, N. M., Flagan, R. C., Hansel, A., Kulmala, M., Lelieveld, J.,
- 1150 Volkamer, R., Kirkby, J., and Winkler, P. M.: Enhanced growth rate of atmospheric particles from sulfuric acid, *ACP*, 20, 7359-7372, 10.5194/acp-20-7359-2020, 2020.
- Thakur, R. C., Dada, L., Beck, L. J., Quéléver, L. L. J., Chan, T., Marbouti, M., He, X.-C., Xavier, C., Sulo, J., Lampilahti, J., Lampimäki, M., Tham, Y. J., Sarnela, N., Lehtipalo, K., Norkko, A., Kulmala, M., Sipilä, M., and Jokinen, T.: An evaluation of new particle formation events in Helsinki during a
- 1155 Baltic Sea cyanobacterial summer bloom, *ACP*, 22, 6365-6391, 10.5194/acp-22-6365-2022, 2022.
- Tröstl, J., Chuang, W. K., Gordon, H., Heinritzi, M., Yan, C., Molteni, U., Ahlm, L., Frege, C., Bianchi, F., Wagner, R., Simon, M., Lehtipalo, K., Williamson, C., Craven, J. S., Duplissy, J., Adamov, A., Almeida, J., Bernhammer, A.-K., Breitenlechner, M., Brilke, S., Dias, A., Ehrhart, S., Flagan, R. C., Franchin, A., Fuchs, C., Guida, R., Gysel, M., Hansel, A., Hoyle, C. R., Jokinen, T., Junninen, H.,
- 1160 Kangasluoma, J., Keskinen, H., Kim, J., Krapf, M., Kürten, A., Laaksonen, A., Lawler, M., Leiminger, M., Mathot, S., Möhler, O., Nieminen, T., Onnela, A., Petäjä, T., Piel, F. M., Miettinen, P., Rissanen, M. P., Rondo, L., Sarnela, N., Schobesberger, S., Sengupta, K., Sipilä, M., Smith, J. N., Steiner, G., Tomé, A., Virtanen, A., Wagner, A. C., Weingartner, E., Wimmer, D., Winkler, P. M., Ye, P., Carslaw, K. S., Curtius, J., Dommen, J., Kirkby, J., Kulmala, M., Riipinen, I., Worsnop, D. R., Donahue, N. M., and
- 1165 Baltensperger, U.: The role of low-volatility organic compounds in initial particle growth in the atmosphere, *Nature*, 533, 527-531, 10.1038/nature18271, 2016.
- Veli-Matti Kerminen, M. K.: Analytical formulae connecting the “real” and the “apparent” nucleation rate and the nuclei number concentration for atmospheric nucleation events, *Journal of Aerosol Science*, 33, 609–622, 2002.
- 1170 Wang, Q., Yan, D., Wang, X., Lu, P., Li, X., and Cao, A.: Research advances in soil fumigants, *Acta Phytopylacica Sinica*, 44, 529-543, 2017.
- Wang, Y. Q.: MeteoInfo: GIS software for meteorological data visualization and analysis, *Meteorological Applications*, 21, 360-368, 10.1002/met.1345, 2014.
- Wang, Z., Zheng, F., Zhang, W., and Wang, S.: Analysis of SO<sub>2</sub> Pollution Changes of Beijing-Tianjin-Hebei Region over China Based on OMI Observations from 2006 to 2017, *Advances in Meteorology*, 2018, 1-15, 10.1155/2018/8746068, 2018.
- 1175 Wehner, B., Siebert, H., Stratmann, F., Tuch, T., Wiedensohler, A., Petäjä, T., Dal Maso, M., and Kulmala, M.: Horizontal homogeneity and vertical extent of new particle formation events, *Tellus B: Chemical and Physical Meteorology*, 59, 362-371, 10.1111/j.1600-0889.2007.00260.x, 2007.



- 1180 Williams, J., Gros, V., Atlas, E., Maciejczyk, K., Batsaikhan, A., Schöler, H. F., Forster, C., Quack, B., Yassaa, N., Sander, R., and Van Dingenen, R.: Possible evidence for a connection between methyl iodide emissions and Saharan dust, *Journal of Geophysical Research*, 112, 10.1029/2005jd006702, 2007.
- Wu, Z., Hu, M., Liu, S., Wehner, B., Bauer, S., Ma Bling, A., Wiedensohler, A., Petäjä, T., Dal Maso, M., and Kulmala, M.: New particle formation in Beijing, China: Statistical analysis of a 1-year data set, 1185 *Journal of Geophysical Research*, 112, 10.1029/2006jd007406, 2007.
- Xiao, M., Hoyle, C. R., Dada, L., Stolzenburg, D., Kürten, A., Wang, M., Lamkaddam, H., Garmash, O., Mentler, B., Molteni, U., Baccharini, A., Simon, M., He, X.-C., Lehtipalo, K., Ahonen, L. R., Baalbaki, R., Bauer, P. S., Beck, L., Bell, D., Bianchi, F., Brilke, S., Chen, D., Chiu, R., Dias, A., Duplissy, J., Finkenzeller, H., Gordon, H., Hofbauer, V., Kim, C., Koenig, T. K., Lampilahti, J., Lee, C. P., Li, Z., 1190 Mai, H., Makhmutov, V., Manninen, H. E., Marten, R., Mathot, S., Mauldin, R. L., Nie, W., Onnela, A., Partoll, E., Petäjä, T., Pfeifer, J., Pospisilova, V., Quéléver, L. L. J., Rissanen, M., Schobesberger, S., Schuchmann, S., Stozhkov, Y., Tauber, C., Tham, Y. J., Tomé, A., Vazquez-Pufleau, M., Wagner, A. C., Wagner, R., Wang, Y., Weitz, L., Wimmer, D., Wu, Y., Yan, C., Ye, P., Ye, Q., Zha, Q., Zhou, X., Amorim, A., Carslaw, K., Curtius, J., Hansel, A., Volkamer, R., Winkler, P. M., Flagan, R. C., Kulmala, 1195 M., Worsnop, D. R., Kirkby, J., Donahue, N. M., Baltensperger, U., El Haddad, I., and Dommen, J.: The driving factors of new particle formation and growth in the polluted boundary layer, *ACP*, 21, 14275-14291, 10.5194/acp-21-14275-2021, 2021.
- Yan, C., Yin, R., Lu, Y., Dada, L., Yang, D., Fu, Y., Kontkanen, J., Deng, C., Garmash, O., Ruan, J., Baalbaki, R., Schervish, M., Cai, R., Bloss, M., Chan, T., Chen, T., Chen, Q., Chen, X., Chen, Y., Chu, 1200 B., Dällenbach, K., Foreback, B., He, X., Heikkinen, L., Jokinen, T., Junninen, H., Kangasluoma, J., Kokkonen, T., Kurppa, M., Lehtipalo, K., Li, H., Li, H., Li, X., Liu, Y., Ma, Q., Paasonen, P., Rantala, P., Pileci, R. E., Rusanen, A., Sarnela, N., Simonen, P., Wang, S., Wang, W., Wang, Y., Xue, M., Yang, G., Yao, L., Zhou, Y., Kujansuu, J., Petäjä, T., Nie, W., Ma, Y., Ge, M., He, H., Donahue, N. M., Worsnop, D. R., Veli-Matti, K., Wang, L., Liu, Y., Zheng, J., Kulmala, M., Jiang, J., and Bianchi, F.: 1205 The Synergistic Role of Sulfuric Acid, Bases, and Oxidized Organics Governing New-Particle Formation in Beijing, *GRL*, 48, 10.1029/2020gl091944, 2021.
- Yang, L., Nie, W., Liu, Y., Xu, Z., Xiao, M., Qi, X., Li, Y., Wang, R., Zou, J., Paasonen, P., Yan, C., Xu, Z., Wang, J., Zhou, C., Yuan, J., Sun, J., Chi, X., Kerminen, V. M., Kulmala, M., and Ding, A.: Toward Building a Physical Proxy for Gas-Phase Sulfuric Acid Concentration Based on Its Budget Analysis in 1210 Polluted Yangtze River Delta, East China, *EST*, 55, 6665-6676, 10.1021/acs.est.1c00738, 2021.
- Yang, X., Xiao, D., Bai, H., Tang, J., and Wang, W.: Spatiotemporal Distributions of PM<sub>2.5</sub> Concentrations in the Beijing–Tianjin–Hebei Region From 2013 to 2020, *Frontiers in Environmental Science*, 10, 10.3389/fenvs.2022.842237, 2022.
- Yao, L., Garmash, O., Bianchi, F., Zheng, J., Yan, C., Kontkanen, J., Junninen, H., Mazon, S. B., Ehn, 1215 M., Paasonen, P., Sipilä, M., Wang, M., Wang, X., Xiao, S., Chen, H., Lu, Y., Zhang, B., Wang, D., Fu, Q., Geng, F., Li, L., Wang, H., Qiao, L., Yang, X., Chen, J., Kerminen, V.-M., Petäjä, T., Worsnop, D. R., Kulmala, M., and Wang, L.: Atmospheric new particle formation from sulfuric acid and amines in a Chinese megacity, *Science*, 361, 278-281, 10.1126/science.aao4839, 2018.
- Yokouchi, Y., Nojiri, Y., Toom-Saunty, D., Fraser, P., Inuzuka, Y., Tanimoto, H., Nara, H., Murakami, 1220 R., and Mukai, H.: Long-term variation of atmospheric methyl iodide and its link to global environmental change, *GRL*, 39, n/a-n/a, 10.1029/2012gl053695, 2012.

- Yokouchi, Y., Osada, K., Wada, M., Hasebe, F., Agama, M., Murakami, R., Mukai, H., Nojiri, Y., Inuzuka, Y., Toom-Saunty, D., and Fraser, P.: Global distribution and seasonal concentration change of methyl iodide in the atmosphere, *Journal of Geophysical Research*, 113, 10.1029/2008jd009861, 2008.
- 1225 Zhang, R., Xie, H. B., Ma, F., Chen, J., Iyer, S., Simon, M., Heinritzi, M., Shen, J., Tham, Y. J., Kurtén, T., Worsnop, D. R., Kirkby, J., Curtius, J., Sipilä, M., Kulmala, M., and He, X. C.: Critical Role of Iodous Acid in Neutral Iodine Oxoacid Nucleation, *Environ Sci Technol*, 56, 14166-14177, 10.1021/acs.est.2c04328, 2022.
- 1230 Zhou, Y., Hakala, S., Yan, C., Gao, Y., Yao, X., Chu, B., Chan, T., Kangasluoma, J., Gani, S., Kontkanen, J., Paasonen, P., Liu, Y., Petäjä, T., Kulmala, M., and Dada, L.: Measurement report: New particle formation characteristics at an urban and a mountain station in northern China, *ACP*, 21, 17885-17906, 10.5194/acp-21-17885-2021, 2021.